CHALMERS

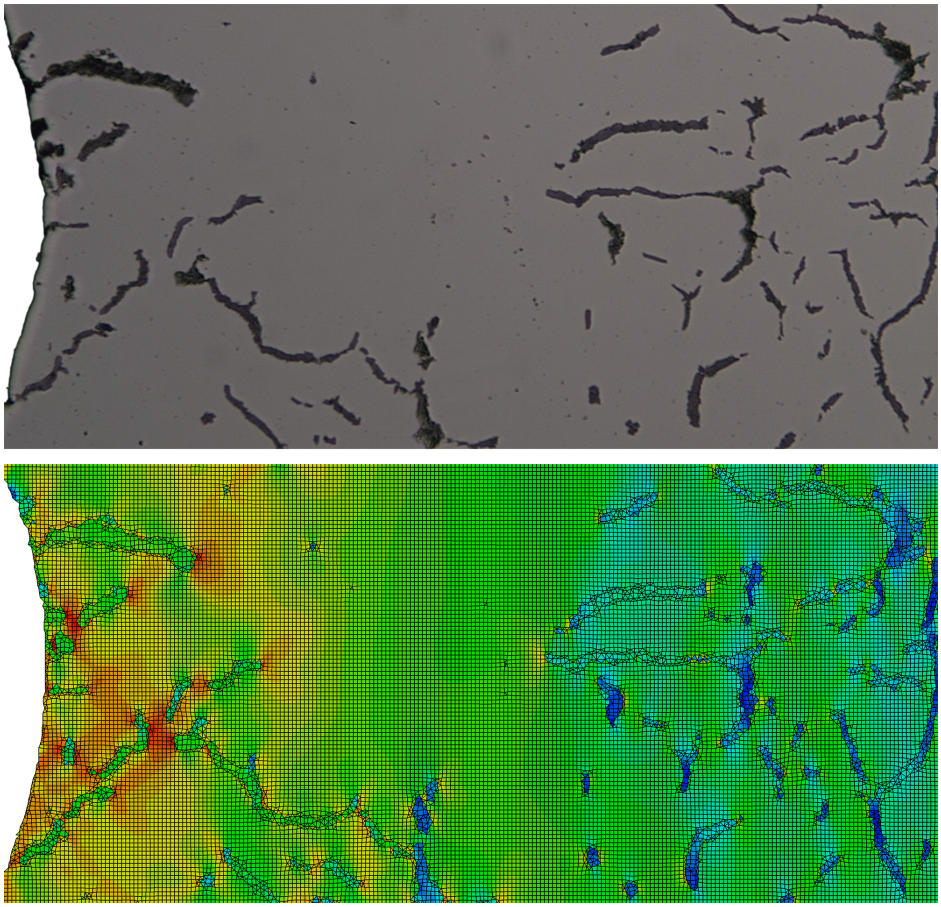

Analysis and modeling of properties of Compacted Graphite Iron on a microstructural level

Master's thesis in Applied Mechanics

PETER HELLSTRÖM
KIM OLANDER

Department of Applied Mechanics
Division of Material and Computational Mechanics
CHALMERS UNIVERSITY OF TECHNOLOGY
Gothenburg, Sweden 2012
Master's thesis 2012:08

MASTER'S THESIS IN APPLIED MECHANICS

Analysis and modeling of properties of Compacted Graphite Iron on a microstructural level

PETER HELLSTRÖM
KIM OLANDER

Department of Applied Mechanics
Division of Material and Computational Mechanics
CHALMERS UNIVERSITY OF TECHNOLOGY
Gothenburg, Sweden 2012

Analysis and modeling of properties of Compacted Graphite Iron on a microstructural level
PETER HELLSTRÖM
KIM OLANDER

Master's thesis 2012:08
ISSN 1652-8557
Department of Applied Mechanics
Division of Material and Computational Mechanics
Chalmers University of Technology
SE-412 96 Gothenburg
Sweden
Telephone: +46 (0)31-772 1000

Cover:
Image of CGI microstructure and corresponding FE-discretization.

Chalmers Reproservice
Gothenburg, Sweden 2012

Analysis and modeling of properties of Compacted Graphite Iron on a microstructural level
Master's thesis in Applied Mechanics
PETER HELLSTRÖM
KIM OLANDER
Department of Applied Mechanics
Division of Material and Computational Mechanics
Chalmers University of Technology

Abstract

This master thesis deals with finding material parameters for the Johnson-Cook (JC) fracture and hardening model in order to obtain a realistic representation of the deformation and fracture response of Compacted Graphite Iron (CGI). The parameters are needed when simulating e.g. machining processes of CGI in order to optimize and receive a better knowledge of the process and the influence of the microstructure. In the fracture model, only influence from the stress triaxiality component is analyzed, whereas in the hardening model, only the isotropic strain hardening component is analyzed. Thus, the contribution from strain rate and temperature dependence is omitted. Furthermore, two cases are considered: In the first case, CGI is treated as a homogeneous material, not taking into account the two entering constituents, pearlite and graphite. In the second case, the actual heterogeneity of CGI is considered, taking the morphology of the two constituents into account by explicitly including them in the finite element (FE) analyses.

To find the material parameters, tensile tests have been conducted on flat test specimens with four different notch geometries. For the fracture model, the fracture strain is of interest whereas for the hardening model the entire stress-strain curve is needed. The strains are obtained by the use of a Digital Image Correlation (DIC) system. In addition to this, FE-analyses are conducted on the same geometries, from which the stress triaxiality in the fracture zone is computed and used as input to the fracture parameter calibration. The data from the tensile tests and the FE-analyses are imported into Matlab where optimization scripts utilizing the non-linear least square method are used to find the parameters in the JC-material models.

From the FE-analyses force-strain curves are obtained, which are compared to the respective experiments for all four geometries. The results for the homogeneous approach agree well and the parameters from optimization seem reasonable. It should be remarked that, during the project, several assumptions are made in terms of e.g. plane stress and the location of crack initiation. These may influence the final JC-parameters and it is concluded that further investigation is needed to validate the results. For the heterogeneous approach, initial studies have been made and they show that the method used works, but further investigation is needed.

Keywords: Compacted Graphite Iron, CGI, Johnson-Cook, Fracture model, Parameter calibration, Finite element method, Tensile testing, Digital Image Correlation, DIC

Preface

This thesis in solid mechanics is the final part of a two year Master of Science program in Applied Mechanics at Chalmers University of Technology. It is also the final part of a five year education in Mechanical Engineering. The work has been carried out at Chalmers University of Technology and at SP Technical Research Institute of Sweden during the period January 2012 - June 2012.

We would like to express our gratitude to our supervisors Prof. Lennart Josefsson, Dr. Martin Fagerström and PhD-student Goran Ljustina at the Division of Material and Computational Mechanics at Chalmers University of Technology, and to Dr. Torsten Sjögren at SP Technical Research Institute of Sweden, for their help and guidance during this project. We would also like to thank all PhD-students and other employees at both Chalmers and SP for their kind assistance and patience with our many questions.

Finally, we would like to give a special thanks to PhD-student Erik Lindfeldt at the Division of Material and Computational Mechanics at Chalmers University of Technology for inspiring us to choose a thesis within this subject.

Göteborg, June 2012

Peter Hellström
Kim Olander

Contents

Abstract i

Preface iii

Contents v

1 Introduction 1
1.1 Background . . . 1
1.2 Purpose . . . 1
1.3 Method . . . 1
1.3.1 Homogeneous approach . . . 1
1.3.2 Heterogeneous approach . . . 2
1.4 Limitations . . . 2

2 Theoretical background 3
2.1 CGI in manufacturing industry . . . 3
2.2 The Johnson-Cook model . . . 3
2.3 Digital Image Correlation (DIC) . . . 5
2.4 Finite element method . . . 6
2.4.1 Element removal technique . . . 6
2.4.2 Mass scaling . . . 7
2.4.3 Sub-modeling . . . 7

3 Tensile and shear tests 8
3.1 Material . . . 8
3.2 Specimen design . . . 8
3.3 Experimental procedure . . . 9
3.3.1 Test preparation . . . 9
3.3.2 Tensile testing machine . . . 10
3.3.3 DIC analysis . . . 10

4 FE-modeling 13
4.1 Homogeneous material approach . . . 13
4.1.1 Mesh creation . . . 13
4.1.2 Setup and solving . . . 13
4.1.3 Acquiring results . . . 14
4.2 Heterogeneous material approach . . . 14
4.2.1 Mesh creation . . . 14
4.2.2 Setup and solving . . . 15
4.2.3 Acquiring results . . . 15

5 Parameter Optimization 16
5.1 Homogeneous approach . . . 16
5.1.1 Parameters in hardening model . . . 16
5.1.2 Parameters in fracture model . . . 16
5.2 Heterogeneous approach . . . 16

6 Results 17
6.1 Homogeneous approach . . . 17
6.1.1 Mechanical testing . . . 17
6.1.2 FE-analysis . . . 20
6.1.3 Parameter optimization . . . 20
6.1.4 Comparison and validation . . . 22
6.2 Heterogeneous approach . . . 23

6.2.1 FE-analysis . . . 23
6.2.2 Parameter optimization . . . 23

7 Discussion **24**
7.1 The Johnson-Cook model . . . 24
7.2 Tensile testing . . . 24
7.2.1 Fracture strain . . . 24
7.2.2 Strain fields . . . 24
7.2.3 Crack propagation . . . 24
7.2.4 Miscellaneous sources of error for tensile testing . . . 24
7.3 FE-modeling . . . 25
7.3.1 Simulated crack propagation . . . 25
7.3.2 Heterogeneous FE-simulations . . . 25
7.3.3 Miscellaneous sources of error for FE-modeling . . . 25
7.4 Comparison and validation . . . 26
7.4.1 Homogeneous parameters . . . 26
7.4.2 Heterogeneous parameters . . . 27
7.5 General discussion . . . 27
7.5.1 Methodology . . . 27
7.5.2 Sustainability . . . 27

8 Conclusions **28**

9 General recommendations and future work **29**
9.1 Strain rate and temperature dependence . . . 29
9.2 Alternative specimen design . . . 29
9.3 Improved FE-modeling . . . 29
9.4 Tensile tests and DIC-analysis . . . 29
9.5 FEA with DIC . . . 30

References **31**

Appendices

A Test specimen drawings **I**
A.1 Shear notch geometry . . . I
A.2 Large radius notch geometry . . . III
A.3 Circular notch geometry . . . V
A.4 Triangular notch geometry . . . VII

B Matlab Codes **VIII**
B.1 ADdataFromAramisFinal.m . . . VIII
B.2 EMakingFinal.m . . . IX
B.3 ParamOptimJCModelHetero.m . . . X
B.4 ParamOptimJCModelsHomo.m . . . XI
B.5 JCFractureFunction.m . . . XIII
B.6 JCHardeningFunction.m . . . XIII
B.7 AbaqusShearEdtv2.m . . . XIV

C Tensile testing machine specifications **XVI**

1 Introduction

There are several reasons to study Compacted Graphite Iron (CGI). One reason is the increasing use of the material in manufacturing processes of, e.g. the engine blocks of trucks, where the properties of CGI are well suited as it combines some of the properties of gray cast iron and ductile iron. When designing and simulating the machining process, these properties need to be well defined. Compared with conventional grey cast iron, CGI increases the opportunities to reduce wall thickness at current operating loads due to its higher strength, reduce cylinder bore distortion and improve noise, vibration and harshness properties etc [1]. The potential reduction of component weight and increased efficiency in production decreases the environmental impact. When using simulations, instead of multiple equivalent real world experiments, the time and energy consumed as well as the loss of material in machining processes is reduced, motivating this study of CGI from both an environmental and economical perspective. This contributes to a strive of sustainable development. CGI has become commercially viable as reliable methods of production have been developed therefore increasing its use. The material is not as thoroughly studied as other materials that have been in greater commercial use for a long time. Therefore additional analysis would be interesting from both an academic point of view and for industrial applications.

The possibility to study materials using so called Digital Image Correlation (DIC), which is a contactless measurement technique, is increasing as computational capacities increase and digital images have higher quality. This technique uses sequentially recorded images at different applied loads or strains. By comparing these images, the strain level in different parts of the microstructure can be determined. To be able to make this comparison between the images, it is assumed that the material has a pattern which can be used to measure displacements. It is essential that there is enough resolution and contrast differences in the pattern. One of the advantages with the technique is that while loading a specimen, not only are the average deformations measured but also the localized strain at e.g. welds and other disturbances in the material, and how different phases deform in multiphased materials. One example of when DIC has been used can be found in e.g. [2].

1.1 Background

SP Technical Research Institute of Sweden (SP) utilizes a DIC-system, Aramis [3], for contactless deformation measurements. This system is mainly used for measurements on component and specimen level. However, in recent projects a methodology has been developed to measure on a microscopic level with images sampled through a microscopy system during loading of the specimen. In this Master's Thesis project, the DIC-system and tensile testing equipment are used to study a CGI alloy and its deformation behavior, with emphasis on fracture. The deformation mechanisms that can be identified on a microscopic level will be correlated to the global deformation in order to gain an increased understanding of the macroscopic deformation behavior, with particular emphasis on the fracture mechanical properties of the material.

There are currently a number of ongoing projects at the Department of Applied Mechanics at Chalmers University of Technology dealing with mechanical modeling and simulation of machining processes of CGI, e.g. [4]. In these projects, the fracture characteristics of CGI plays an important role.

1.2 Purpose

The main purpose of this thesis is to study the deformation and fracture of CGI. Parameters for the Johnson-Cook (JC) fracture and hardening model [5], considering CGI as a homogeneous material, will be determined and the deformation behavior will be analyzed.

In addition to this, a heterogeneous approch is considered where the contribution from the entering phases (graphite and pearlite) in deformation and fracture is studied.

1.3 Method

1.3.1 Homogeneous approach

In the homogeneous approach, CGI as a material is considered to be completely homogeneous and only one constitutive model is needed to describe the response to loading and fracture. To be able to determine

the parameters of the JC-hardening model and the JC-fracture model, for the homogeneous approach, the deformation and stress states are needed. The deformation is found by conducting tensile tests along with DIC. As the stress state, specially the triaxiality, varies with different load cases i.e specimen geometry, four different geometries are used in the tensile test to produce the experimental results needed in form of strain fields and axial load. Finite Element (FE) simulations, performed in the FE-software Abaqus FEA [6], are later used to determine the triaxiality for each load case. The combined values from experiments and simulations are then used to determine the JC-parameters via optimization scripts in Matlab R2011b [7]. The results are then updated and the triaxiality is checked once again to determine if any large change occurs when the new parameters are used.

1.3.2 Heterogeneous approach

For the heterogeneous approach, the material of the test specimen is considered to contain two constituents, pearlite and graphite. Each constituent is described by its own constitutive model, in which the equation for JC-hardening and JC-fracture model exist, doubling the number of material parameters needed. The JC-hardening parameters used in this work are taken from the literature [8]. The experiments produce strain fields and crack propagation paths as well as images of the microstructure that in turn are used to create an FE-mesh. The simulations based on these meshes are used to determine the triaxiality in local areas along crack propagation paths. Once again, the fracture strain and triaxiality are combined and JC-fracture parameters are determined via optimization, this time for the microstructural constituents, focusing on pearlite.

1.4 Limitations

The master thesis work has been carried out during the spring of 2012. In this thesis, the only material model used is the Johnson-Cook model. The strain-rate and temperature dependence in the model was however not taken into account. Only two-dimensional representations assuming plane stress are used for FE-simulation. Data was only gathered from the surface of the models due to the limitations of DIC. Only one type of CGI, CGI 500, was investigated. For the heterogeneous approach, only the fracture parameters for pearlite are sought. The work with DIC was conducted at SP Technical Research Institute of Sweden (SP) in Borås whereas simulations and optimization was preformed at Chalmers University of Technology.

2 Theoretical background

This chapter presents the theoretical background that forms the basis of this thesis. First, the CGI material in general is described, its properties and how it relates to other materials. Following this description, the Johnson-Cook material model is explained. The chapter continues with an introduction to the use of DIC and concludes with explanations of some special techniques in FE-modeling that are used in this project.

2.1 CGI in manufacturing industry

Higher demands on engine efficiency and lowered emissions due to economy and legislation can be satisfied by new engine designs. For heavy duty machines, such as diesel truck engines, increasing bore pressures put greater stress on the material in cylinder blocks, liners, and heads. The materials in these components need to withstand the wear and tear of combustion pressures as high as 200 bar [9].

The commercial use of CGI for these applications is relatively new if compared to grey cast iron and common aluminum alloys. Also, the mechanical properties of CGI are not as well documented. The beneficial properties of CGI are mostly due to its microstructure, an interconnected worm-like form of graphite embedded into a pearlite dominated matrix. The structure of the graphite can be seen in Figure 2.1. In contrast, ordinary grey cast iron has sharp graphite flakes in a lamellar structure. The latter results in a high thermal conductivity, but because of the sharp geometry of the graphite flakes, areas with high stress concentrations are created within the microstructure making grey cast iron a brittle material. This brittleness of grey cast iron results in good machinability. Nodular cast iron on the other hand has spherical nodules of graphite with no interconnections making it ductile and strong, but a poor heat conductor and more difficult to machine [10].

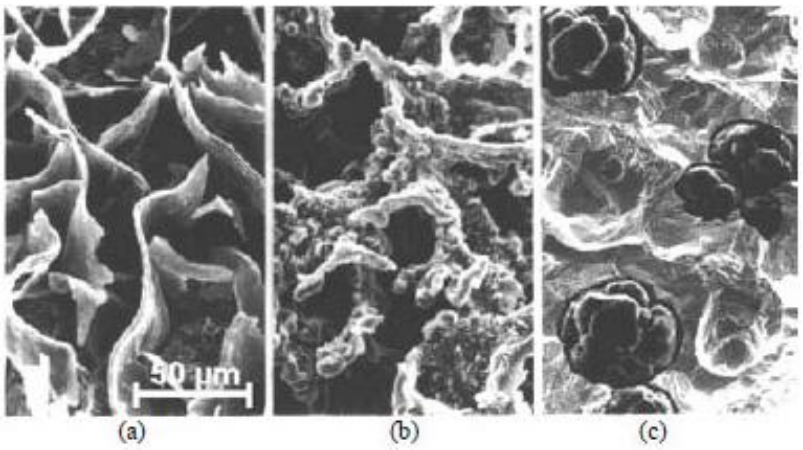

Figure 2.1: *Graphite morphology in grey (a), compact (b) and ductile (c) iron. Image from [11].*

CGI combines some of the thermal properties and the machinability of grey cast iron with the strength and ductility of nodular cast iron, resulting in properties between those of grey- and nodular cast iron, which makes it ideal for engine components. By controlling the cooling rate and mixture in certain areas of a component, different zones of mechanical properties can be created.

2.2 The Johnson-Cook model

Simulation of large plastic deformations and fracture in solid mechanics can be handled by several different material models. The material model consists of three parts. A linear model used to describe elastic behavior, a hardening model describing the plastic hardening and a fracture model that determines when fracture occurs. These parts are usually phenomenological models with parameters based on experiments. In the linear elastic region, the isotropic Hooke's law is the simplest possible way to describe deformation. When dealing with plastic deformation non-linear material models are usually implemented to capture the plastic behavior, such as kinematic and isotropic hardening effects of the material. When the material finally fails, a fracture model is

needed to describe this. The simplest way is to use a constant fracture model [12] where the fracture strain ϵ_f is constant regardless of load case. The constant fracture model is simple to calibrate and implement but for more complex loading cases this might be insufficient. There are several other fracture models such as the Wilkins approach, the maximum shear stress approach, the Cockcroft–Latham approach and the Bao–Wierzbicki approach, with varying complexity and applicability [12]. One reason to choose the Johnson–Cook fracture model over the other above mentioned models is its common use in high speed, high deformation simulations such as machining. There are also several projects in progress at Chalmers University of Technology where the Johnson-Cook fracture and hardening models are used.

The Johnson-Cook constitutive model, proposed 1983 [5] together with a later addition of a fracture model, is a material model using in total 13 parameters to model large plastic deformations and fracture criteria. The three key material responses are strain hardening, strain-rate effects, and thermal softening. They can be seen in that order in equation (2.1) where $\overline{\sigma}$ represents the yielding and hardening behavior. The Johnson-Cook cumulative-damage fracture model is an extension of the original model that adds the possibility to model fracture and can be seen in equation (2.2) where ϵ_f is the fracture strain.

$$\overline{\sigma} = \underbrace{\left[A + B\left(\epsilon^p_{eff}\right)^N\right]}_{\text{Strain hardening}} \cdot \underbrace{\left[1 + C\ln\dot{\epsilon}\right]}_{\text{Strain rate dep.}} \cdot \underbrace{\left[1 - (T_H)^M\right]}_{\text{Thermal softening}} \tag{2.1}$$

$$\epsilon_f = \underbrace{\left[d_1 + d_2 e^{d_3\sigma^*}\right]}_{\text{Stress triaxiality}} \cdot \underbrace{\left[1 + d_4\ln\dot{\epsilon}\right]}_{\text{Strain rate dep.}} \cdot \underbrace{\left[1 + d_5 T_H\right]}_{\text{Temperature dep.}} \tag{2.2}$$

The strain rate is defined as $\dot{\epsilon} = \frac{\dot{\epsilon}^p_{eff}}{\dot{\epsilon}_0}$ where $\dot{\epsilon}_0$ is the strain rate used to determine the variables A, B and N, and $\dot{\epsilon}^p_{eff}$ is the effective plastic strain rate [13]. The homologous temperature used in the last part of the equations expresses the temperature as a fraction of the melting temperature $T_H = \frac{T - T_R}{T_M - T_R}$. Here T_M is melting temperature and T_R is the reference temperature used to determine the constants.

The present study focuses on slow loading at room temperature, hence the focus of this work is on the first part of equations (2.1) and (2.2), related to strain hardening and stress triaxiality respectively, where the three constants d_1, d_2 and d_3, as well as A, B and N are determined using different load cases and specimen geometries. d_1 is the initial failure strain, d_2 is the exponential factor and d_3 is the triaxiality factor [14]. A is interpreted as the yield stress whereas B and N represents the effect from strain hardening [5].

It is commonly known that a hydrostatic tensile stress state promotes void growth in a ductile material, which accelerates the fracture process. Consequently, the stress triaxiality influences ductility by lowering the fracture strain limit for high values of triaxiality [15], as seen in Figure 2.2. Stress triaxiality is defined as the negative pressure, $-P$, divided by von Mises stress, σ_{vM}, see equation (2.3).

$$\sigma^* = \frac{-P}{\sigma_{vM}}, \quad P = \frac{\sigma_{kk}}{3} \tag{2.3}$$

The triaxiality varies with different geometries and load cases, as visualized in Figure 2.2, and the local area studied in each case has a specific triaxiality. The variation of triaxiality is a part of what is used to determine the three constants for the Johnson-Cook fracture model.

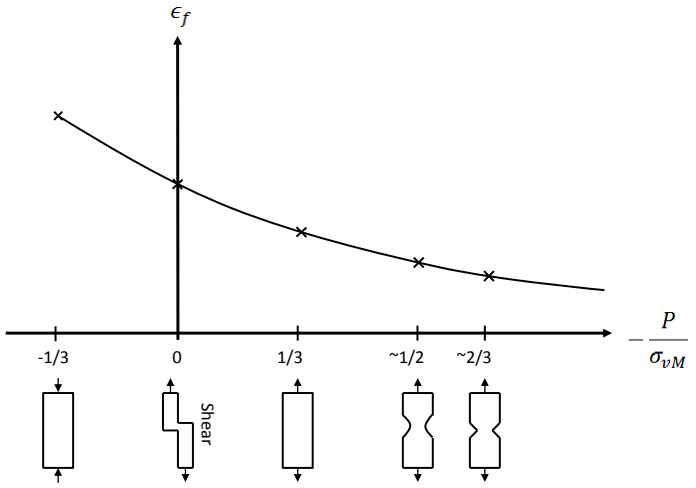

Figure 2.2: *An illustrative example of triaxiality vs failure strain for JC fracture model.*

2.3 Digital Image Correlation (DIC)

DIC is a method to track changes in a series of images, e.g. deformation of a surface, by optical tracking of unique features in the images. DIC works by capturing images during different stages of deformation and then post-processing the resulting data in a dedicated software. One advantage of the DIC method is its non-invasive properties and the ability to capture large deformations as well as local strains. One disadvantage is that only the surface of the object is studied. This can be overcome by using X-ray tomography together with Digital Volume Correlation (DVC), however this method is far more costly and the equipment has not been available for this thesis.

DIC works by matching sub-regions of consecutive images. The sub-regions, also called facets, are defined in the software and the size is determined by the properties of the object of study. Each facet must be unique and contain several pixels of different grey- or color levels, as seen in Figure 2.3. Figure 2.4 shows a representative image of the facets appearance in the Aramis software. This can be achieved either by the objects material structure, e.g. microstructure, or by applying a random pattern to the object.

The size of the facets influences the spatial resolution and the strain resolution of the data, i.e. how small changes in strain can be detected. Large facets give low spacial resolution but high strain resolution, and vice versa. Large facets are also more likely to be unique and thus tracking ability is improved. Using too small facets might cause some of them to appear in areas with limited variation in greyscale thus making them hard to uniquely identify. Facets can also overlap to create more reliable results.

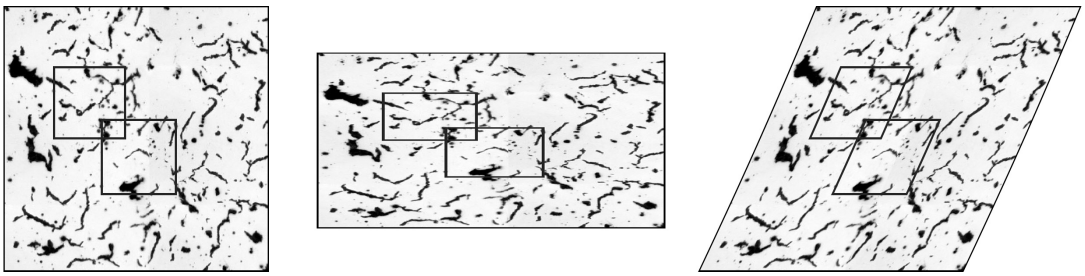

(a) *Original image* (b) *Elongation* (c) *Shear*

Figure 2.3: *The overlapping squares depict facets used for DIC in three different cases. In this case a the CGI microstructure is used as the random pattern.*

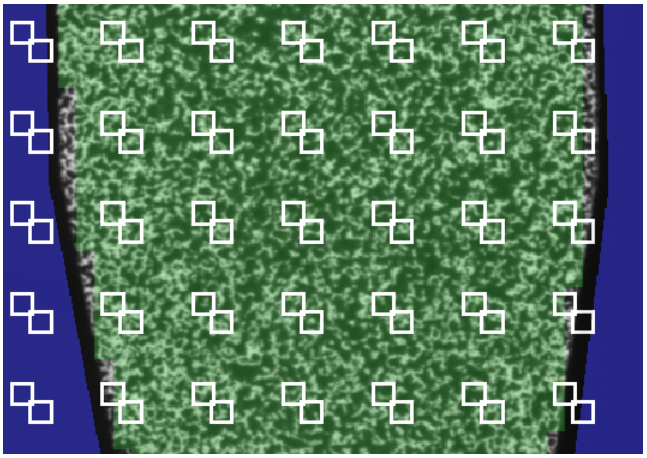

Figure 2.4: *A representative image of the facet appearance in the Aramis software showing a selection of the facets used. In this case black and white spray paint is used as the random pattern.*

2.4 Finite element method

2.4.1 Element removal technique

The element removal technique is a simple way of simulating crack propagation in FE-analysis. The technique states that an element should be removed from the analysis when a certain condition is fulfilled. In this case, the condition is that if the accumulated effective plastic strain divided by the fracture strain reaches one, see equation (2.4), the element is removed. The technique is further described in [14].

$$D = \sum \frac{\Delta \epsilon^p_{eff}}{\epsilon_f} \text{ , failure occurs when } D = 1 \tag{2.4}$$

Mesh dependent crack propagation

Mesh-size affects the response of the structure studied. A fine mesh results in less plastic deformation before fracture than a coarse mesh, when using the element removal technique. These effects seem to be more pronounced for low strain rates.

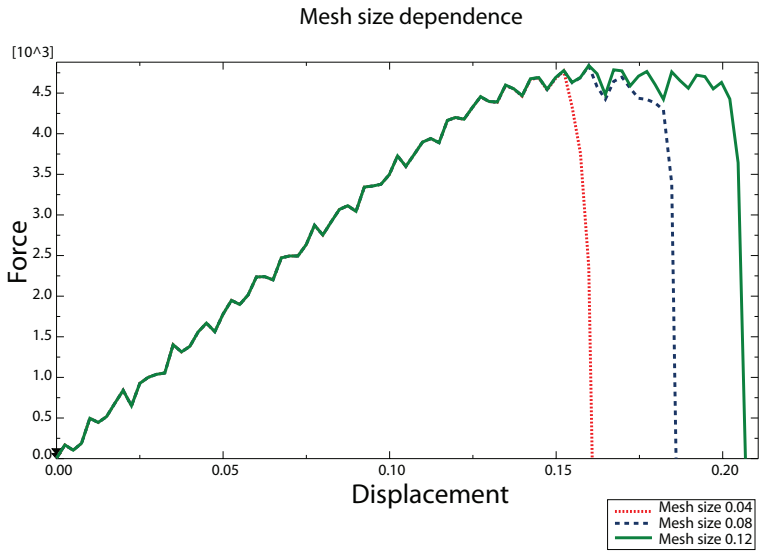

Figure 2.5: *Mesh size dependence, showing the force and displacement needed to fracture a simulated notched bar.*

2.4.2 Mass scaling

Mass scaling increases the mass of the elements to improve the time step in explicit simulations [16]. Improvement in this case means that a larger time step can be used, which decreases the total computational time. The critical time step is limited by the highest eigenfrequency, ω_{max}, of the system $\Delta t_c = \frac{2}{\omega_{max}}$ and proportional to $\Delta t_c \sim \frac{h}{c}$, where h is the characteristic element size and $c \sim \sqrt{\frac{k}{\rho}}$ the wave propagation speed proportional to element stiffness and density. This relation is strictly valid only for an elastic material. An increase of mass lowers the eigenfrequency and raises the wave propagation speed. The increase of mass is suitable for quasi-static load cases, as in this project, or low frequency problems. For high-frequency response, eigenvalue problems or other problems where dynamics are especially important, the increased mass might influence the response of the system significantly [17].

2.4.3 Sub-modeling

Sub-modeling is a technique that allows the user to analyze one specific area of a structure with higher accuracy, while allowing the whole structure to be simulated with lower accuracy. This is a suitable way to save computational time. Sub-modeling works by first running a simulation of the whole structure with a coarse mesh. The results from this simulation are then used as input, e.g. boundary condition, for a higher accuracy simulation of the subdomain of interest. More information can be found in e.g. [18]. This technique has been used in the heterogeneous approach.

3 Tensile and shear tests

In this section, the tensile tests are explained. A short description of the CGI used in the experiments and of the specimen design is given. The experimental procedure including test preparation, the tensile testing machine and the DIC system is also described.

3.1 Material

The CGI used in the tensile test is CGI 500 [19]. Most CGI materials contain some fraction of ferrite, however the CGI used in this project has almost none and the simulations will not take the ferrite into account. Mechanical properties and material composition can be seen in Table 3.1 and Table 3.2, respectively. An image of the microstructure can be seen in Figure 3.1.

Table 3.1: CGI 500 mechanical properties according to ISO16112:2006.

Ultimate tensile strength	Young's Modulus	Density	Poisson's ratio
500 to 575 MPa	145 to 160 GPa	7 to 7.2 g/cm^3	0.26

Table 3.2: CGI 500 specimen material composition.

C: 3.53 wt%	Si: 2.08 wt%	Mn: 0.27 wt%	P: <0.005 wt%	S: 0.013 wt%	Cr: 0.03 wt%
Ni: 0.02 wt%	Mo: <0.01 wt%	Cu: 0.84 wt%	Sn: 0.084 wt%	Ti: 0.005 wt%	V: 0.005 wt%

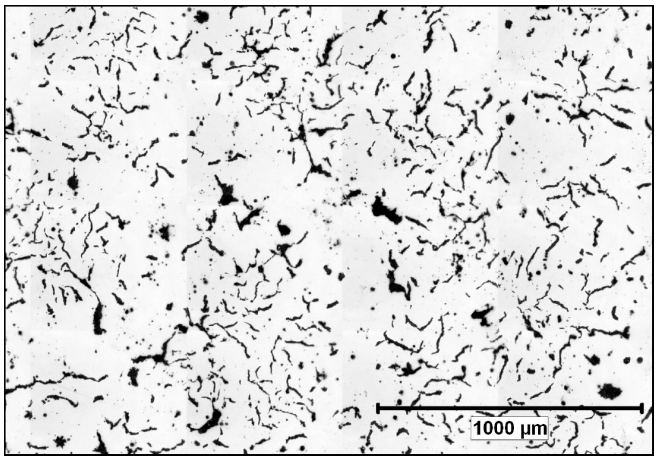

Figure 3.1: *Microstructure of the CGI 500 material used in testing. Light material is pearlite, dark material is graphite.*

3.2 Specimen design

The limitation of the tensile testing equipment to only create uniaxial displacement means that the sample geometry determines the fracture locus. To get the best conditions to find the parameters for the fracture criteria, a wide range of stress triaxiality values are needed. Since the triaxiality varies with load case and geometry, a number of test specimens with different notch geometries were created. Elastic FE-analyses performed in Abaqus [6] gave the results in Table 3.3 for the different geometries at the areas where fracture is most likely to occur. After these initial simulations, and consultation with the supervisors, four different notch geometries were chosen. The geometries can be seen in Figure 3.2. Drawings of the test specimens were created using a CAD software and can be seen in appendix A.

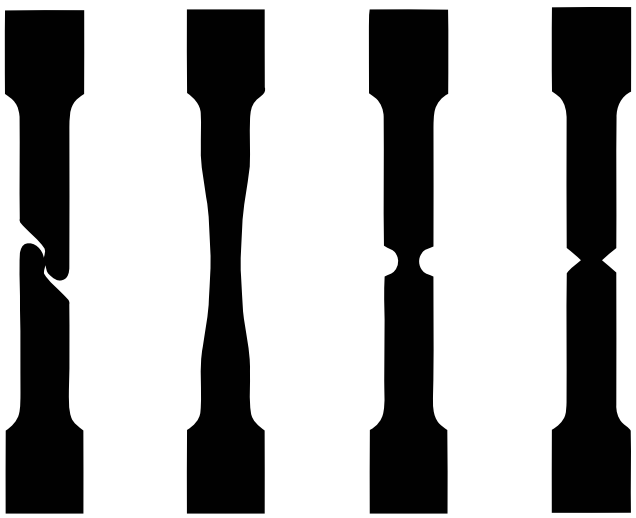

Figure 3.2: *Geometries for the different test specimen. From left to right: Shear, Large radius notch, Circular notch, Triangular notch. The effect on triaxiality can be seen in Figure 2.2*

Table 3.3: Geometry and corresponding triaxiality

Geometry	Shear	Large radius notch	Circular notch	Triangular notch
Triaxiality $\left(\frac{-P}{\sigma_{vM}}\right)$	-0.02	0.33	0.49	0.63

3.3 Experimental procedure

GOM's Aramis system [20] is used to perform DIC at SP. The system utilizes two high resolution cameras to capture a series of images of the test object during testing. When the testing is complete, the images are analyzed using correlation analysis [3]. The two cameras are originally intended to analyze three dimensional deformation when used together. In the tests in this project however, one camera will be used together with a microscope to capture the microstructure deformation on one side of the test specimen. At the same time, the other camera will capture the global deformation at the other side of the test specimen. This setup allows gathering and analysis of more data from each test. As mentioned in section 2.2 only the strain hardening and stress triaxiality are studied, therefore the strain rate and temperature are held fixed through out the tensile test phase. The ambient temperature was $T_R = 21$ °C and the strain rate $\dot{\epsilon}_0 = 3 \cdot 10^{-4}$ s^{-1}.

3.3.1 Test preparation

To get high contrast images of the specimen surface needed for DIC, the specimen is prepared in two different ways depending on the image magnification. On the side of microscope imaging, the surface is polished in several steps to reveal the color difference between graphite and pearlite and to achieve the high contrast needed. If the magnification is too high, or if the microstructure contains large areas of pearlite without any graphite, the surface contains no unique features for the DIC-process to identify in that area. This means that the system can not calculate the displacement field there. To create more unique features, the surface is either etched with a 3% nital solution and/or toner powder from a printer is added. The fine toner powder adheres to the surface and creates additional high contrast features [19]. On the other surface, facing the camera without a microscope, a stochastic gray scale pattern is applied using matte white and black spray paint, see Figure 2.4.

3.3.2 Tensile testing machine

The tensile testing machine at SP used in these experiments is developed to fit the DIC system. It is designed for tests where the microstructure deformation is studied. The maximum loading capacity of the machine is 10 kN, specifications can be found in appendix C. A load cell connected to the DIC-system is located at the bottom of the sample holder. The data from this load cell is collected and together with the strains computed by the DIC-software, stress-strain curves are created. The main advantage with this specialized machine is the manner in which the grips are symmetrically displaced. This assures that the center of the specimen stays stationary and minimizes any lateral movement. The use of a microscope in testing means that any lateral movement of the specimen would cause a shift out of the microscope's focal plane resulting in image blur.

In Figure 3.3 the tensile testing machine can be seen together with the two Aramis cameras. Figure 3.3a shows the first camera used to capture the global deformation of the test specimen and Figure 3.3b shows the second camera mounted on the microscope.

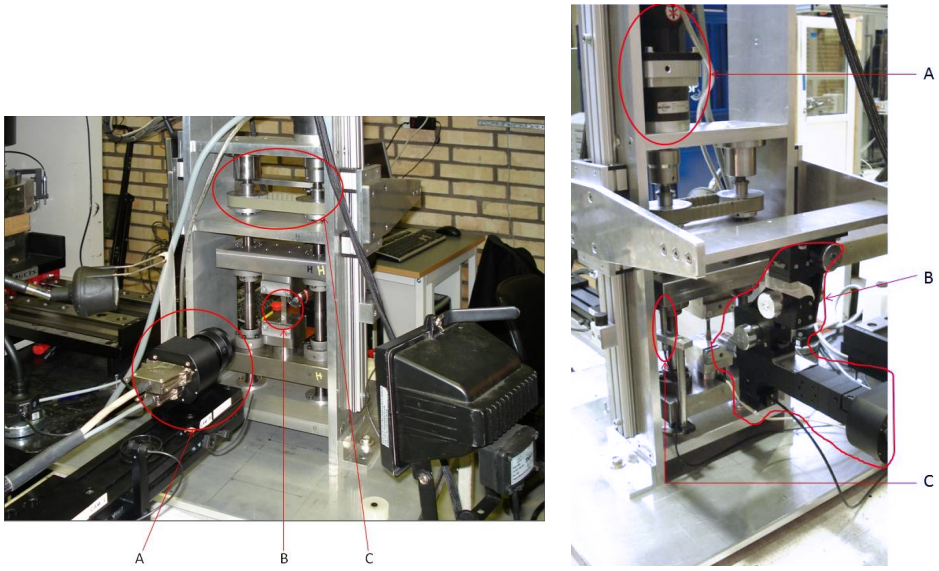

(a) *A) Camera used to capture global deformation field. B) Test specimen with attachment. C) Gears and belt to transfer power from motor.*

(b) *A) Motor and gearbox powering the testing machine. B) Camera and microscope setup. C) Displacement measuring gauge.*

Figure 3.3: *Tensile tensile test machine and cameras used for DIC.*

Direct lighting on the side for global deformation image capturing would result in overexposure in specular highlights. To avoid this, a matte white reflector is rigged to reflect diffuse light from the light source onto the specimen, creating an even lighting.

3.3.3 DIC analysis

Homogeneous approach

With the images collected from testing, a displacement field is computed. In the DIC-software it is possible to place virtual one dimensional strain gauges between two points in the images of the specimen surface. By introducing these virtual strain gauges aligned with the loading at the crack location, the logarithmic strain throughout the test as well as the fracture strain ϵ_f can be calculated for the three cases of large radius, circular, and triangular notch as seen in Figure 3.5. By synchronizing the load output from a load cell with each image the sought time of fracture can be found. Due to the brittle properties of the material, no necking occurs and a steep drop in load is observed when fracture occurs. Therefore, the time of fracture is in this work defined as the time of maximum recorded load [21].

The above mentioned method of strain calculation is not possible for shear cases. The fracture strain for

the shear specimens in this work is calculated by studying the deformation of a quadrangle [2] which is placed over the crack, see Figure 3.6. By computing the angle difference, using equation (3.1), between the sides for the deformed and undeformed quadrangle, see Figure 3.4, the shear angle γ_{12} can be calculated according to equation (3.2) when assuming small angles.

$$cos(\alpha) = \frac{a1 \cdot a2}{|a1||a2|}, \quad cos(\beta) = \frac{b1 \cdot b2}{|b1||b2|} \tag{3.1}$$

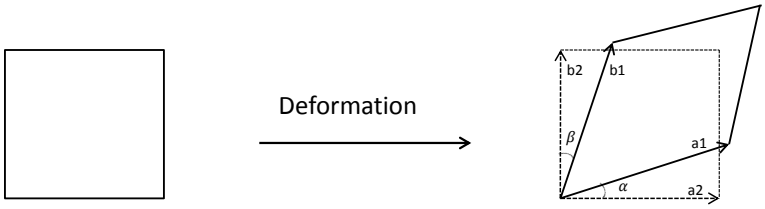

Figure 3.4: *Angles used to compute the shear angle*

$$\gamma_{12} = \alpha + \beta \tag{3.2}$$

When the shear angle is calculated, the matrix representation for the strain tensor $\underline{E}$ for plane stress can be calculated from equation (3.3). For the shear case ϵ_{11}, ϵ_{22} and ϵ_{33} are zero. From the strain tensor, the effective von Mises strain is calculated according to equation (3.4). The fracture strain, ϵ_f, is once again considered to occur when the force recorded during testing reaches its peak.

$$\underline{E} = \begin{bmatrix} \epsilon_{11} & \gamma_{12} & 0 \\ \gamma_{12} & \epsilon_{22} & 0 \\ 0 & 0 & \epsilon_{33} \end{bmatrix} \tag{3.3}$$

$$\epsilon_{vM} = \sqrt{\frac{2}{3}\underline{E}_{dev} : \underline{E}_{dev}} \tag{3.4}$$

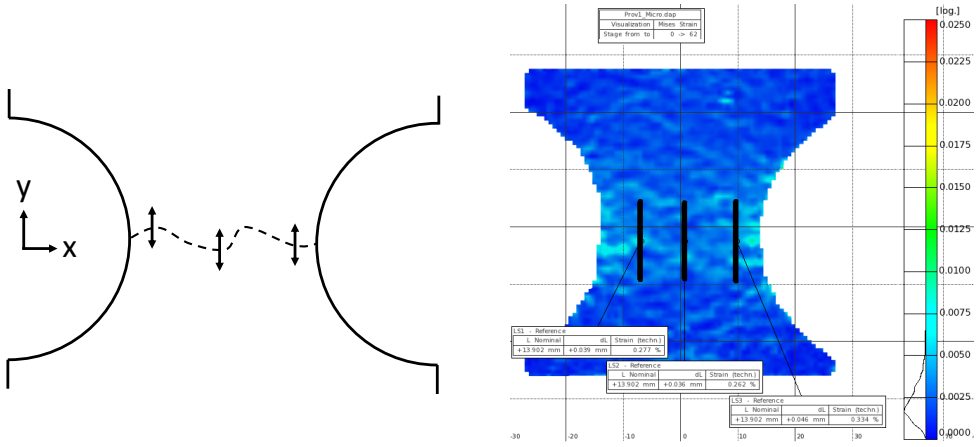

(a) *Representative image of the three virtual strain gauges position in the fracture zone.*

(b) *The virtual strain gauges appearance in the Aramis software.*

Figure 3.5: *Virtual strain gauges used to compute the strain in the tension cases.*

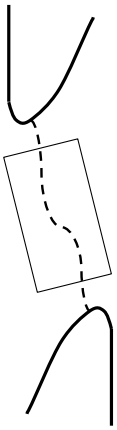

(a) *Representative image of quadrangle over crack.*

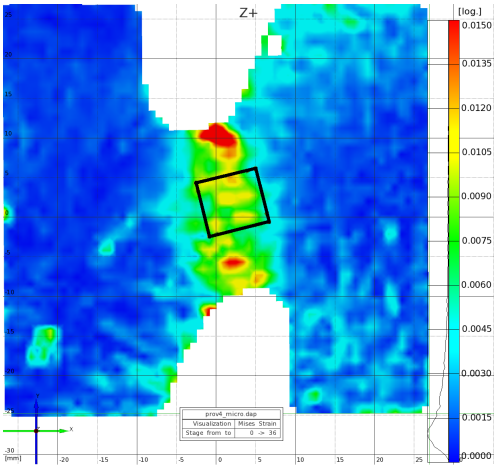

(b) *Quadrangles appearance in the Aramis software.*

Figure 3.6: *Quadrangles used to determine the strain for the shear notch geometry.*

Heterogeneous approach

In the heterogeneous approach, areas with only pearlite are of interest. To find the parameters in the JC fracture model, the fracture strain is needed. This means that the area of interest is where the crack path lies in the pearlite. Since the high magnification microscope in the DIC equipment only covers a small part of the test specimen, the probability of capturing images of the crack is low. To increase this probability, the triangular notch specimen is used since it has the most localized stress and therefore a well controlled fracture locus. This makes it easier to aim the camera at an area where the crack is likely to occur.

When the tensile tests have been performed and the image series have been analyzed, strain information is extracted in pearlitic regions where cracks occur, see Figure 3.7.

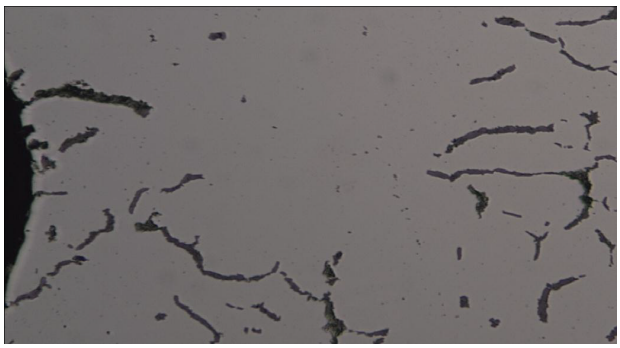

(a) *An image before any toner powder is applied.*

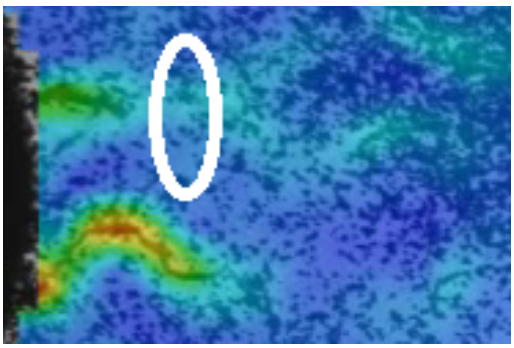

(b) *An image after DIC analysis. Von Mises strain fields with the white circle depicting an area in which strains are extracted.*

Figure 3.7: *Strain field from the DIC-software next to an image of the microstructure.*

4 FE-modeling

In this chapter, the steps in the FE-modeling are described. First the FE-modeling in the homogeneous approach is described, how the mesh is created and how the simulation is set up. Finally, the FE-modeling of the heterogeneous approach is described in the same sequence.

4.1 Homogeneous material approach

The main goal with the homogeneous modeling is to compute the stress triaxiality state in the fracture zone of each test specimen. In addition, for validation of the model, force-strain curves are to be compared with the experiments. The simulation results enable, together with the results from experiments, a way to identify the Johnson-Cook parameters for the material as a whole.

4.1.1 Mesh creation

When creating the FE-mesh for the homogeneous approach, the microstructure's appearance is not taken into account. The mesh is created in Abaqus CAE. The mesh only consists of quadratical elements since triangular elements need very small time-steps and have lower accuracy compared to quadratical elements. The element type is CPS4R, a four node under-integrated bilinear plane stress quadrilateral element. In an attempt to lower the mesh's influence, between the geometries, on the results, the same element size for the smallest elements are used for all four geometries, see subsection 2.4.1. Since the shear notch geometry contains the smallest radius, it formed the basis for the size selection. The smallest elements are approximately 0.05 mm. An example of the mesh for the circular notch geometry can be seen in Figure 4.1.

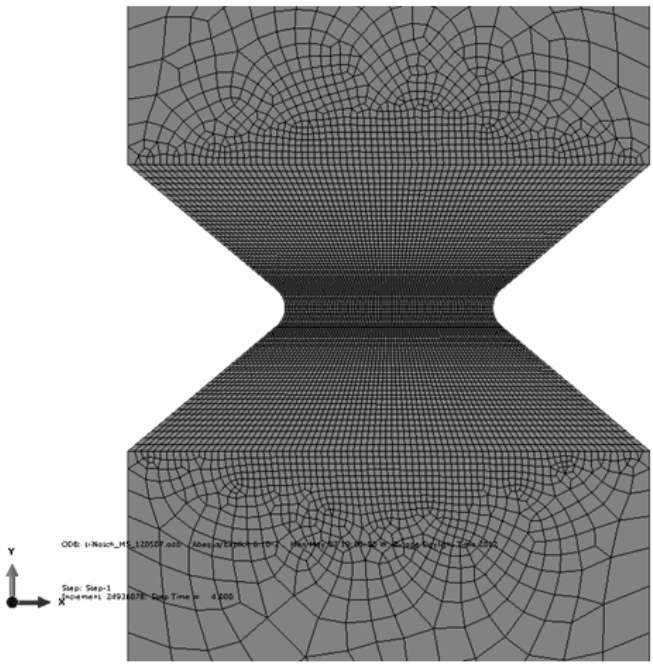

Figure 4.1: *Example of homogeneous FE-mesh.*

4.1.2 Setup and solving

To be able to simulate the crack propagation and fracture using the JC model, the explicit solver in Abaqus CAE is used. This solver uses an explicit central-difference time integration rule and is commonly used for non-linear problems.

Since the models contain small elements, due to the geometry, the possible time step used for explicit integration is also small. This increases the number of steps needed and causes the total computational time to

increase. A way to solve the finite element problem within a reasonable time is to implement mass scaling, see subsection 2.4.2.

As these analyses can be seen as quasi-static, mass scaling is used to shorten the computational time. This is implemented by using Abaqus semi-automatic mass scaling with a target time increment to 10^{-7} s resulting in an increase of mass by 2 to $4.7 \cdot 10^7$ % depending on the geometry in question. The target time is found by conducting several FE-simulations and comparing if the added mass affects the results. The target time selected yields a sufficient decrease of computational time whilst, at the same time, still giving a reasonable solution, see Figure 6.6 and the discussion in section 7.4. The crack is simulated by use of element removal technique, as described in subsection 2.4.1.

4.1.3 Acquiring results

As mentioned earlier, the results of interest for the FE-simulations are stress triaxiality and force-strain curves. Irrespective of the specific specimen design chosen, the stress triaxiality at free boundaries, such as the local notch roots, is always $\sigma^* \approx 0.33$ when assuming plane stress. This corresponds to uniaxial loading [21]. This means that taking the triaxiality values at the free boundaries would not result in representative data. Therefore, the stress triaxialities are taken in the center of the notch region where the crack occurs. The reaction force is taken from the top nodes of the specimen. To be able to compare the force-strain curves from simulation and experiments, the strain is computed in the same fashion in the FE-simulation as in the experiments. This means that information about the vertical displacement of nodes above and below the crack path is extracted. This is done at three different locations similar to the procedure described in subsection 3.3.3. For the shear case, the displacements of four nodes representing the corners of an imaginary quadrangle are extracted corresponding to the method used in the DIC analyses in subsection 3.3.3.

4.2 Heterogeneous material approach

The heterogeneous approach is based on images of the microstructure from tensile test samples. The main goal for the heterogeneous simulations is to compute the triaxiality at fracture locations in the pearlite structure. These areas are identified by studying the image series from tensile test experiments.

4.2.1 Mesh creation

The program used for mesh creation is OOF2 [22]. Creation of a mesh based on an image of the microstructure uses the difference in gray scale between graphite and pearlite to assign regions, in this case the graphite and pearlite phases. Then, an initial quadratic mesh is overlain onto the image. In the next step, nodes are moved to the boarders of each region which distorts the mesh. During this process, some triangular elements might be added in order for the mesh to better follow the microstructure. The last step is to refine the mesh and reassign certain nodes to avoid severely distorted elements. The mesh is then imported into Abaqus and used in regions of interest. The resulting mesh and original image can be seen in Figure 6.7.

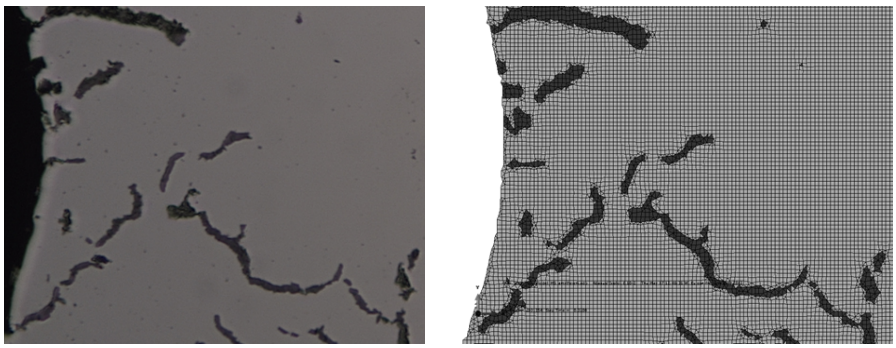

(a) *Image of original microstructure.* (b) *Mesh of microstructure.*

Figure 4.2: *Mesh based on microstructure.*

4.2.2 Setup and solving

The same method of mass scaling and element removal, as in subsection 4.1.2, is used for the heterogeneous model, resulting in a total mass increase of 2 to $4 \cdot 10^7$ % depending on the geometry in question. The difference is that sub-modeling, see subsection 2.4.3, is used to prescribe boundary conditions along the border of the heterogeneous sub-model, see Figure 4.3. This means that the prescribed displacement of nodes on the border is based on the displacement field from the homogeneous simulations. This reduces the time needed to compute the results compared to if the whole model was simulated with such a fine mesh. The sub-modeling also avoids problems that occur if the fine heterogeneous mesh were to be integrated with a coarse homogeneous mesh and the transition between the two. The parameters used for the heterogeneous approach are based on the assumption that graphite is a very brittle material compared to pearlite. It is common to chose parameters for graphite such that it fractures as soon as plasticity starts [8]. To achive this, the parameters d_1 and d_2 are set very low. The other parameters used can be seen in Table 4.1 and 4.2 and are taken from [4].

Table 4.1: Parameters for Graphite in JC model.

Young's modulus	Density	Poisson's ratio	A	B	N	d_1	d_2	d_3
25 GPa	2.56 g/cm^3	0.2	125 MPa	1010 MPa	0.47	0.001	0.001	9.85

Table 4.2: Parameters for Pearlite in JC model.

Young's modulus	Density	Poisson's ratio	A	B	N	d_1	d_2	d_3
190 GPa	7.85 g/cm^3	0.3	522 MPa	525 MPa	0.018	0.0144	0.685	9.85

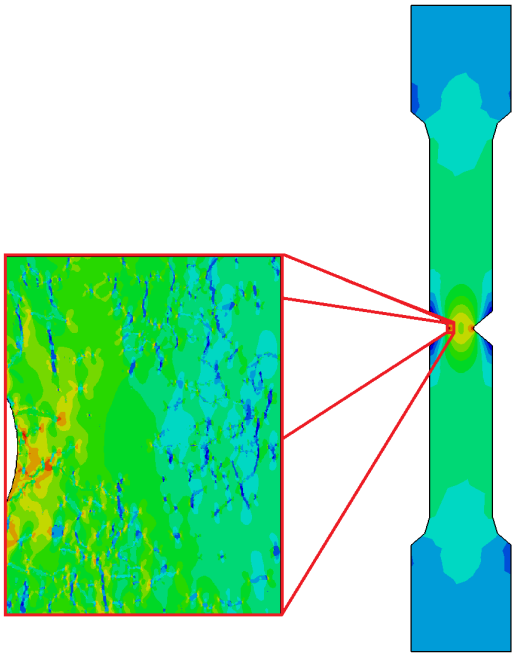

Figure 4.3: *Example on the use of sub modeling.*

4.2.3 Acquiring results

From these FE-simulations, only the triaxiality value of certain points are of interest. These values are taken at the same locations as the strains were taken in the DIC analyses.

5 Parameter Optimization

In this section, the optimization procedure to find the material parameters for the JC-model is described. The optimization are carried out in Matlab using an optimization toolbox. The procedure for the optimization is similar to the one described in [12]. For more information about the optimization toolbox, see Matlab documentation [7].

5.1 Homogeneous approach

5.1.1 Parameters in hardening model

In the hardening model, equation (2.1), there are five unknowns that should be determined, when only considering the effect of strain hardening and not strain rate and temperature dependence. These are: Young's modulus E, yield stress σ_y, A, B and N. As mentioned in section 2.2, A is interpreted as σ_y. E and σ_y are determined from the stress-strain curve created from the tensile tests of the large radius notched specimens. This curve is created from the force-strain curve mentioned in subsection 3.3.2 by computing the engineering stress, $\sigma = \frac{F}{A_{init}}$, from the recorded force. E is calculated by computing the slope of the stress-strain curve in the elastic region. σ_y is approximated by studying the transition region from elastic to plastic response. When E, σ_y and A are decided, the final two parameters are found by utilizing functions in the optimization toolbox in Matlab. A short script together with a function file was created for this purpose. The scripts can be seen in appendix B. The parameters are found by using the nonlinear least square method minimizing the norm of the residual between the measured and simulated stress-strain curve.

5.1.2 Parameters in fracture model

In the fracture model, equation (2.2), there are three unknowns that should be determined: d_1, d_2 and d_3. Just as for the hardening case, a script and a function file was created for the optimization. Input to the script are the fracture strains from the tensile tests and the stress triaxiality calculated in the FE-simulations. The Matlab scripts can be seen in appendix B.

5.2 Heterogeneous approach

As previously mentioned in section 4.2.2, the hardening parameters for both pearlite and graphite used are taken from the literature [8]. Therefore there was no need for any optimization for these parameters. The input for the fracture parameters on the other hand are taken from the DIC-experiments and FE-simulations in form of fracture strains and stress triaxiality. The optimization script for this case is similar to the one used for the homogeneous approach, see section 5.1.2. The script can be seen in appendix B.

6 Results

In this section, results for the different parts in the thesis will be listed. First the tensile and shear tests result from the SP tests are presented. Next comes the FE-analysis and a comparison between these results and the above mentioned. Finally the parameters for the JC-model are shown.

6.1 Homogeneous approach

6.1.1 Mechanical testing

Tensile and shear tests

For the homogeneous approach, five tests were conducted on each of the different geometries. In Table 6.1 the resulting key numbers are shown for these tests. Figure 6.1 shows the same numbers in a graph. The fifth shear test ruptured at two different locations away from the desired one. As a consequence, no fracture strain could be calculated and the fifth entry is therefore not listed. As mentioned in subsection 3.3.3 the fracture strain for the shear case is said to occur when the force reaches its peak value.

The resulting von Mises strain fields from DIC, equation (3.4), can be seen in Figure 6.2. These strain fields are taken from the image just before final fracture for all four geometries. As seen in the image, the heterogeneous nature of CGI influences the strain response even though observing at a relatively low magnification.

Table 6.1: Results from tensile and shear test at SP

Geometry:	**Test nr:**	**Fracture strain [log]:**	**Fracture Force [kN]:**
Shear notch	1	0.0483	0.865
	2	0.0504	0.853
	3	0.0671	0.908
	4	0.0626	0.883
	5	x	x
	Mean value	0.0571	0.88
Large Radius notch	1	0.0167	4.67
	2	0.0164	4.60
	3	0.0170	4.89
	4	0.0223	5.00
	5	0.0172	4.84
	Mean Value	0.0179	4.80
Circular notch	1	0.0218	3.25
	2	0.0160	3.38
	3	0.0125	3.28
	4	0.0172	3.35
	5	0.0187	3.37
	Mean value	0.0172	3.33
Triangular notch	1	0.0081	3.22
	2	0.0080	3.13
	3	0.0125	3.07
	4	0.0156	3.30
	5	0.0165	3.10
	Mean value	0.0121	3.16

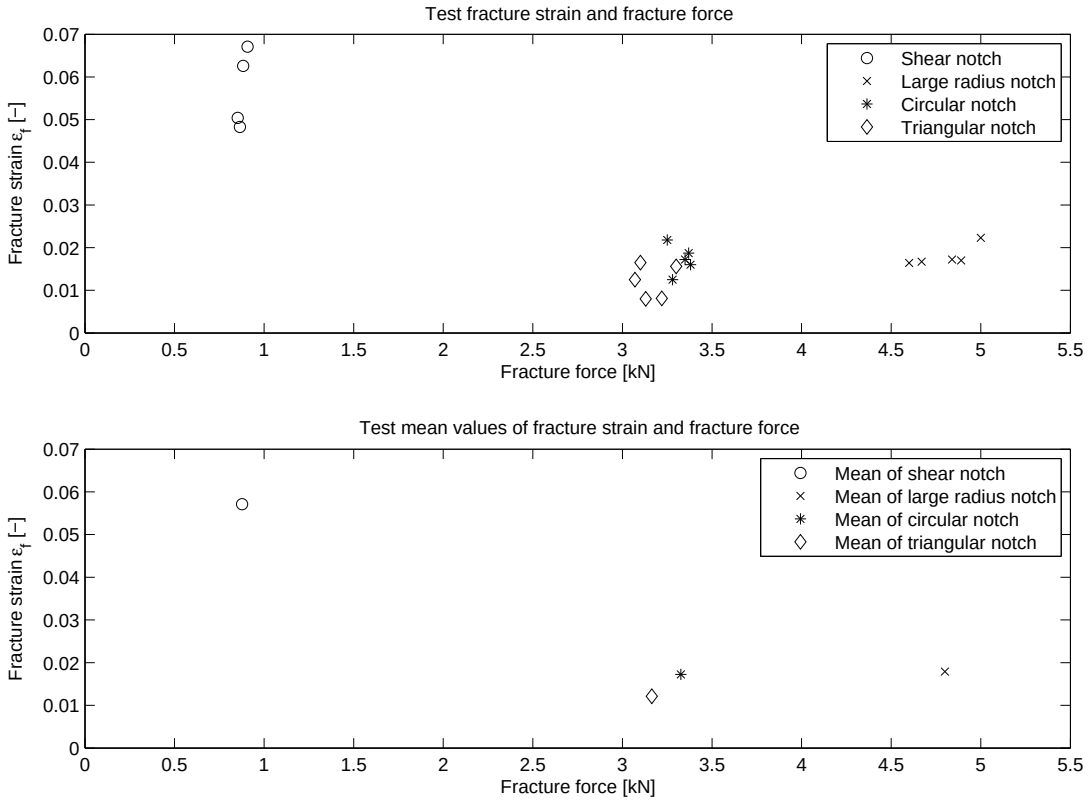

Figure 6.1: *Resulting fracture strain vs fracture force for the tensile tests.*

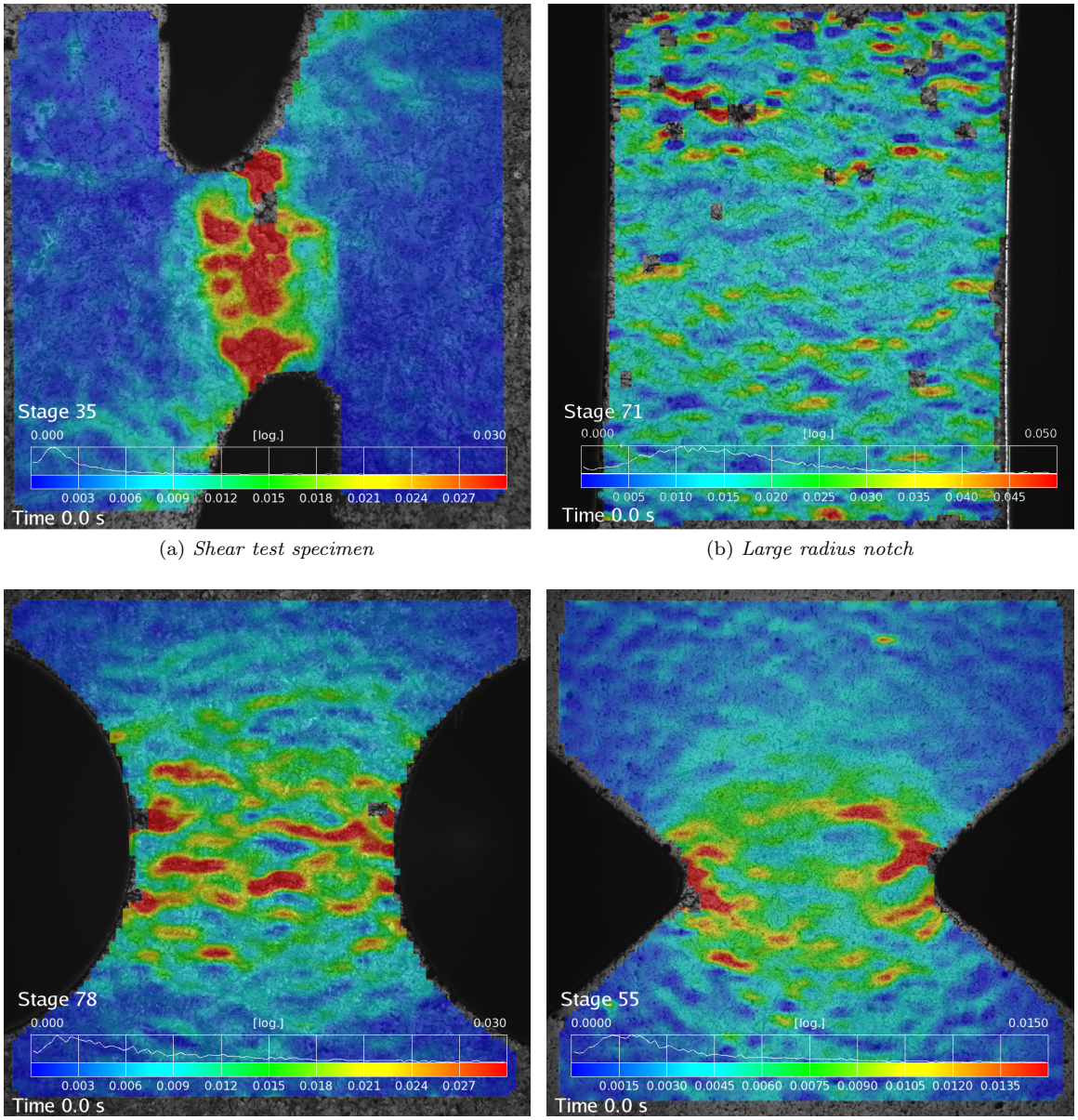

(a) *Shear test specimen*

(b) *Large radius notch*

(c) *Circular notch*

(d) *Triangular notch*

Figure 6.2: *von Mises strain fields from DIC analysis taken from the frame just before fracture.*

Crack propagation

As seen in Figure 6.3, the cracks first appear in the graphite, either as cracks through the interior of the graphite or as decohesion along the boundary between graphite and the pearlite matrix. Initial dislocations as well as fully propagated cracks through the pearlite can be seen originating from the graphite structure.

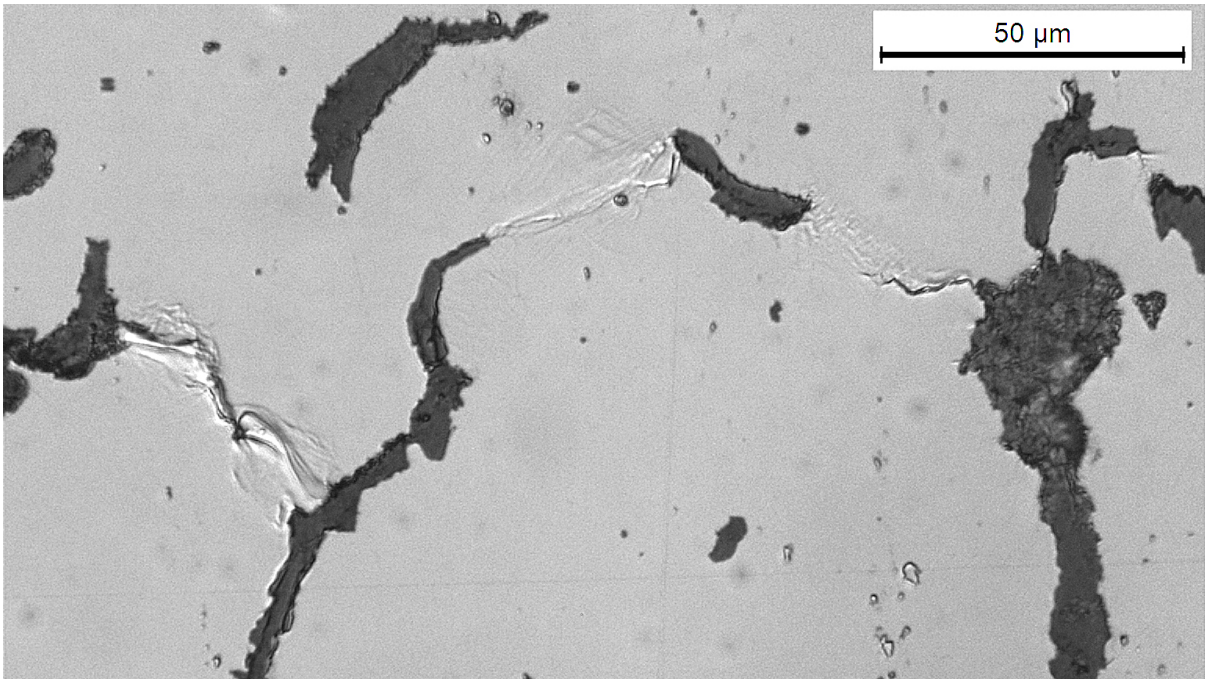

Figure 6.3: *Polished CGI sample after testing with tension in the vertical direction. Graphite appears as dark areas, light areas are pearlite.*

6.1.2 FE-analysis

Triaxiality

Two simulations for each geometry were conducted. The first simulations had JC-parameters taken from [4]. The second simulations had the parameters found by the optimization scripts. The reason for conducting two test was to see if the triaxiality varied too much. The resulting triaxialities can be seen in Table 6.2.

Table 6.2: Resulting triaxialities from FE-simulations.

Geometry	Shear notch	Large Radius notch	Circular notch	Triangular notch
Triaxiality (Simulation 1)	0.048	0.33	0.467	0.603
Triaxiality (Simulation 2)	0.047	0.338	0.467	0.603

6.1.3 Parameter optimization

Hardening

For the JC hardening model, (2.1), the final parameters can be seen in Table 6.3. As mentioned earlier, A is interpreted as the yield stress. In Figure 6.4, the original stress-strain curve, obtained from the tensile tests performed on the large radius notch specimen, together with the JC hardening model can be seen. Based on the original stress-strain curve, the yield stress was approximated to be $\sigma_y = 260$ GPa.

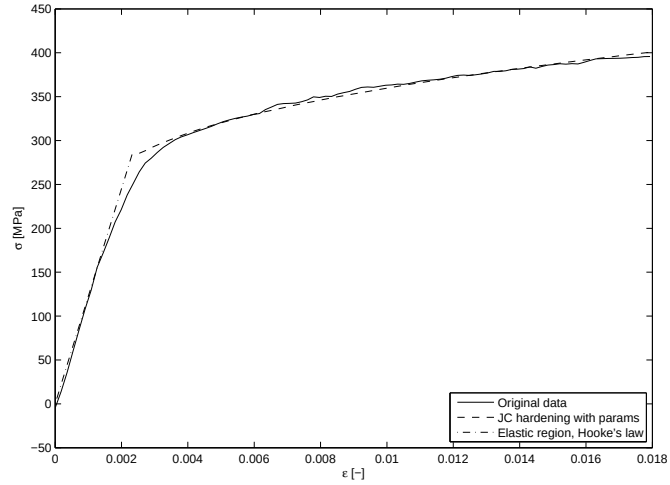

Figure 6.4: *Original stress-strain curve and JC hardening model with resulting parameters. Hooke's law is used in the elastic region.*

Table 6.3: Resulting parameters in the JC hardening model

Parameter	Young's Modulus (E)	Yield Stress (A)	B	N
Value	122.5 GPa	260 MPa	1,01 GPa	0.467

Fracture

For the JC fracture model, (2.2), the final parameters can be seen in Table 6.4. The first row shows the parameters when optimizing against all data points from tensile test experiments and against the stress triaxiality from FE-simulations, i.e. in total 19 data points are used. The second row shows the parameters when optimizing against the mean value of the these data points for each notch geometry, i.e. 4 data points are used. The model is plotted in Figure 6.5 together with the original data points from the experiments. The triaxiality history, that is how the triaxiality varies with the strain up to fracture, is also plotted.

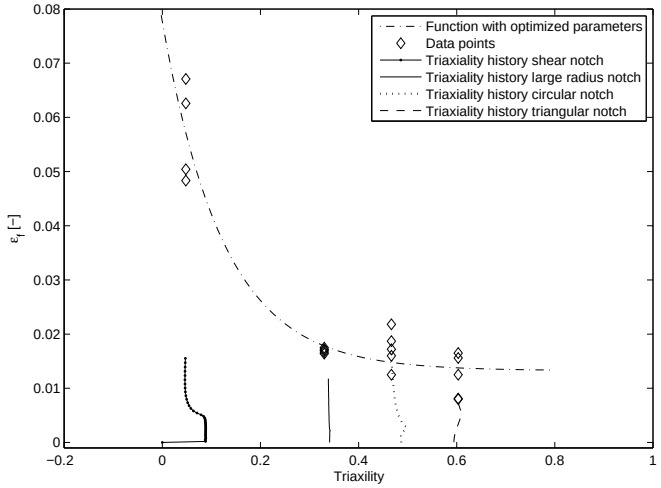

Figure 6.5: *Resulting JC fracture model plotted with optimized parameters together with data points from the experiments and the triaxiality history calculated from FE-simulations.*

Table 6.4: Resulting parameters in the JC fracture model

Parameter	d_1	d_2	d_3
Value (All data points)	0.0133	0.0644	8.023
Value (Mean of data points)	0.0133	0.0645	8.057

6.1.4 Comparison and validation

Figure 6.6 shows the force versus strain curves for the four different geometries. The dotted lines are the averaged results from experiments and the solid lines the results from FE-simulations. The experimental results are truncated at the time of maximum force where, according to the definition, the fracture occurs. The results are discussed further in section 7.4.

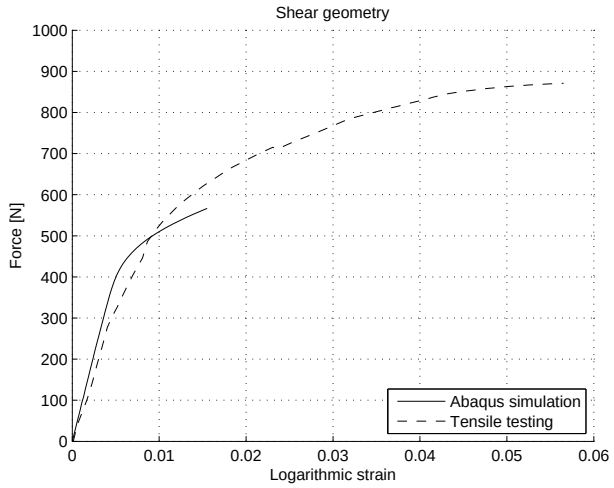

(a) *Shear test specimen*

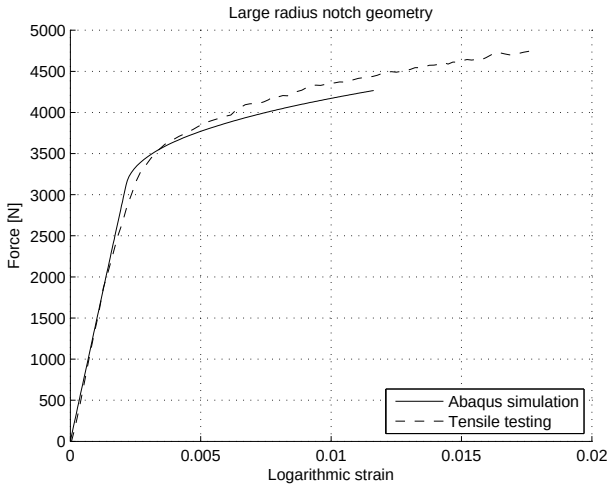

(b) *Large radius notch*

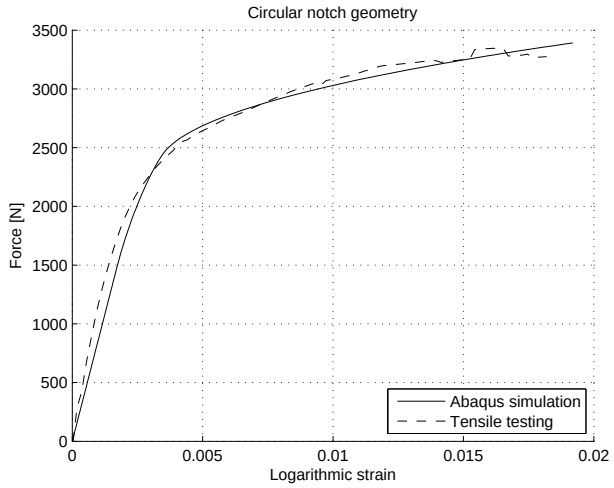

(c) *Circular notch*

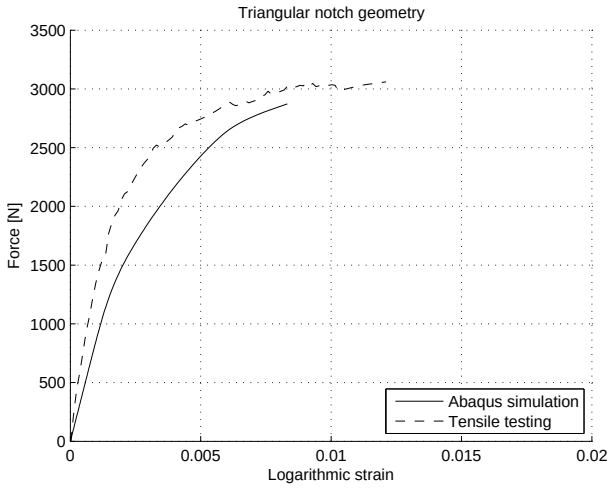

(d) *Triangular notch*

Figure 6.6: *Force-strain curves for the different geometries. The tensile testing curves are averaged from all tests performed for each geometry.*

6.2 Heterogeneous approach

6.2.1 FE-analysis

In Figure 6.7a and 6.7b the microstructure of a heterogeneous sub-model FE-simulation of the triangular notch can be seen. The area shown is 1mm in from the notch root.

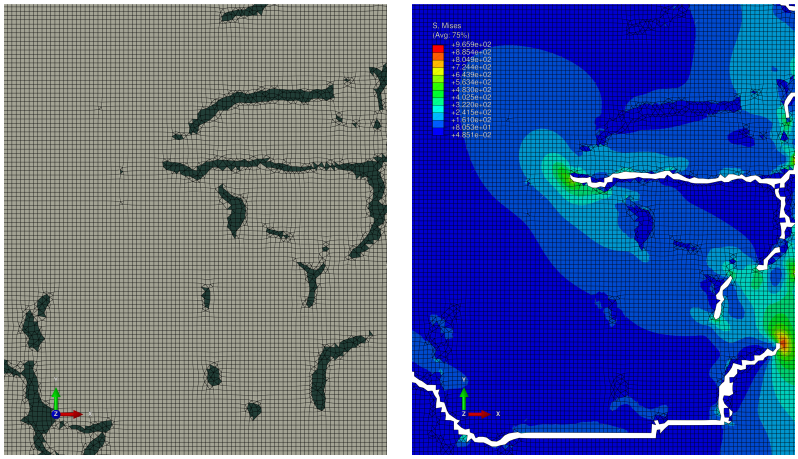

(a) *FE-mesh, graphite represented as dark grey and pearlite as light grey.*

(b) *FE-simulated deformation shown for a load just below the fracture load, based on sub modeling.*

Figure 6.7: *Mesh based on microstructure.*

6.2.2 Parameter optimization

In Figure 6.8 the JC fracture model with optimized parameters is plotted together with the data points used for the optimization.

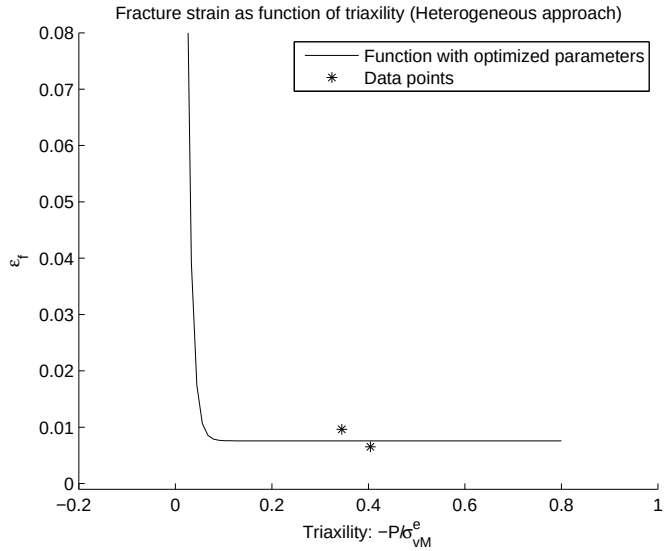

Figure 6.8: *Resulting JC-fracture model for the pearlite phase plotted with optimized constants and data points from tensile tests and FE-simulations.*

7 Discussion

7.1 The Johnson-Cook model

The JC model used in this project provides a direct way to simulate the deformation behavior sought. There are however several phenomenological behaviors that are not possible to recreate using the JC-model. One of these, is the inability to model fracture softening for ductile fractures. Another issue is that the model can not capture the transitional behavior in the yield stress region. This region marks the transition from elastic to plastic behavior. The deviation from experimental data in this region as well as not being able to represent a continuously differentiable curve is thought to have little influence on the results, as seen in Figure 6.4.

7.2 Tensile testing

7.2.1 Fracture strain

Figure 6.1 shows the fracture force and fracture strains for the different tensile tests. As expected, the test specimens with the large radius notch requires the largest force to fracture. This due to the higher stress absorbing area and lower stress concentration. One other observation that can be made is that the fracture strain for the large radius notch and the circular notch is almost identical. It would have been expected that the circular notch should have a lower fracture strain, due to the higher stress concentration because of the notch factor. However, this might be explained by the higher strain in the middle of the notch area compared to the area at the notch root. This increases the mean value of the strains and consequently the fracture, when calculated according to the procedure described in subsection 3.3.3. For the other two tensile geometries, large radius and triangular notch, the reverse is true, i.e. the strains are higher towards the notch roots. This decreases the mean values of the fracture strain for these two geometries. A more suitable approach would have been to use a higher number of virtual gauges across the cross section.

7.2.2 Strain fields

The strain fields shown in Figure 6.2 seem reasonable. The microstructure's influence on the strain is distinct. As the graphite is more brittle than the pearlite, areas with a large fraction of graphite have a higher strain. The areas in red, indicating large strain, in Figure 6.2 contain a lot of graphite. This random microstructural influence motivates the use of several virtual strain gauges to measure the fracture strain, since local effects may influence the strain if only one gauge were to be used.

7.2.3 Crack propagation

Crack propagation through the material microstructure is mostly determined by the geometry of the graphite structure. The cracks first appear in the graphite structure and then propagates from graphite grain to graphite grain via the pearlite. Even though the dominant factor of crack initiation and propagation is the graphite structures geometry, other factors, such as pearlite-pearlite grain boundaries and inclusions, may also have an influence as suggested in [23].

7.2.4 Miscellaneous sources of error for tensile testing

DIC

One obvious disadvantage with the DIC- method is the fact that the test specimens are only studied at the surface. No information is given about the microstructure's appearance inside the specimen. This is especially true for the heterogeneous approach when studying the pearlite. There is no possibility to know if the pearlite studied in DIC is pure pearlite or if there is some graphite just under the surface. This could possibly influence the results in local areas of the heterogeneous tests.

Noise and vibrations

Noise in the measuring equipment and ground vibrations may influence the recorded load and image data. The noise in load data shows up as spikes or drops in the load curves. The spikes forced a manual control of the load data when seeking the maximum force for determination of when fracture occurs to ensure that the correct maximum is found. The DIC-system would interpret vibrations as rigid body movement of the test specimen and this would not influence the strain calculation, however information might be lost at the border of the image

Manufacturing

In order to get the small radii and geometries of the test specimen, a technique called wire discharge machining was used by the workshop who manufactured the test specimens. The technique works by letting a wire with a pulsating current cut the material. Usually the whole sample and equipment is immersed into a liquid, e.g. distilled water, to remove heat and cut off material [24]. It can be seen on the surface of the test specimens that this process has an impact on the material but it is hard to say how large this impact is and how deep into the interior of the specimens it goes.

7.3 FE-modeling

7.3.1 Simulated crack propagation

The method of simulating cracks by the element removal technique tends to influence the cracks propagation. This means that the crack observed in both homogeneous and heterogeneous simulations differ slightly in form of shape and path. The main influence however, is the fact that element removal technique may not be the optimal way to simulate a crack in a brittle material. The technique also shows mesh dependence.

7.3.2 Heterogeneous FE-simulations

The heterogeneous FE-simulation showed a very good agreement with the DIC-analysis. The method of modeling the graphite phase as very brittle have support both in literature and reality. The FE-mesh of the microstructure contains some triangular elements which might be undesirable, c.f. section 4.1.1. However, the use of triangular elements makes the FE-mesh resemble the microstructure's appearance much better. Since it is the heterogeneous nature of CGI that is the focus of the heterogeneous approach, the use of triangular elements is approved from this point of view.

Pearlite-graphite boundary interaction

The interaction between pearlite and graphite at the boundary of each constituent is modeled without any consideration of special interface conditions at present, i.e. as elements in the same mesh and body with different material parameters. The real interaction might be more similar to two separate bodies with defined contact criteria, e.g. friction and adhesion. The appearance of cracks, see Figure 6.3 together with 6.7b, and their propagation suggested that the simple approach without special boundary conditions is sufficient for initial studies like this, but the load response may change and be closer to reality if a more complex approach is made. Such an approach is made in [25] where the decohesion in the graphite-pearlite boundaries is studied and modeled by using inter-cohesive nodes and a damage evolution.

7.3.3 Miscellaneous sources of error for FE-modeling

Plane stress assumption

The plane stress assumption in FE-modeling is valid when one dimension of the structure is very small compared with the others. In this work, the thickness of the test specimen was intended to be that very small dimension. However, due to problem with manufacturing and the characteristics of the CGI, the thickness could not be less than two mm. Since the notch area of the test specimen has a width of approximately three (Circular and Triangular notch) to six (Large radius notch) mm this assumption might not be completely valid. The method of using a flat specimen for testing might also influence the final results as opposed to using a axisymetrical specimen.

7.4 Comparison and validation

7.4.1 Homogeneous parameters

Hardening Parameters

The results based on the parameters found for the JC hardening model seem reasonable. It is shown in Figure 6.4 that the JC hardening model plotted with the resulting parameters from the optimization agrees well with the original data obtained from the tensile tests.

One observation can be made regarding the difference in Young's modulus $E = 122.5$ GPa found in this work, compared with the material data listed in Table 3.1, where $E = 145$ to 160 GPa. This can be explained by the fact that the method of finding the values differ. In this thesis, the tensile test specimens are flat compared with the more common round ones. The strains are also calculated in a different way, normally one mounts strain gauges onto the specimen. In this thesis, the strains are computed based on images and DIC. The length of the virtual strain gauges as well as the fact that it was not possible to use un-notched test specimens might also contribute. An initial test with an un-notched test specimen showed fracture at the mount location.

Fracture parameters

The resulting material parameters in Table 6.4 for the homogeneous approach seem reasonable when considering the three cases of tensile tests. The triaxiality histories seen in Figure 6.5 end close to the spread of the three cases of large radius, circular and triangular notch. This indicates that the fracture parameters are well suited for simulation of tensile load cases, since the fracture strains are similar. The issues with the shear notch simulation are discussed in the section about force-strain curves below.

Force-strain curves

The force-strain curves in Figure 6.6 indicates a good overall agreement between the FE-simulations and the tensile tests. Especially the circular notch geometry shows a good agreement in both shape of the curves and the fracture strain. For the large radius notch and the triangular notch geometries, the shape of the curves are similar but fracture occurs earlier in the FE-simulations. This might be explained by the fact that fracture occurs almost instantly in the FE-simulations due to the element removal technique. The strain measuring in the FE-simulations might also differ slightly compared with the DIC, even if the methods are similar as described in sections 3.3.3 and 4.1.3. The shear geometry shows a large difference in fracture strain. Studies of the images from the tensile tests of the shear geometry shows that the crack growth is more ductile and there exists a force absorbing part some times after the initiation of the crack, see Figure 7.2. This is however not the case in the FE-simulation, showing a very brittle responce. When the crack starts, the crack growth is fast and fracture is almost instantaneous, see Figure 7.1. This is the main reason for the difference in fracture strain. There may also be an other possible explanation in the uncertainty of the fracture parameters regarding shear load cases.

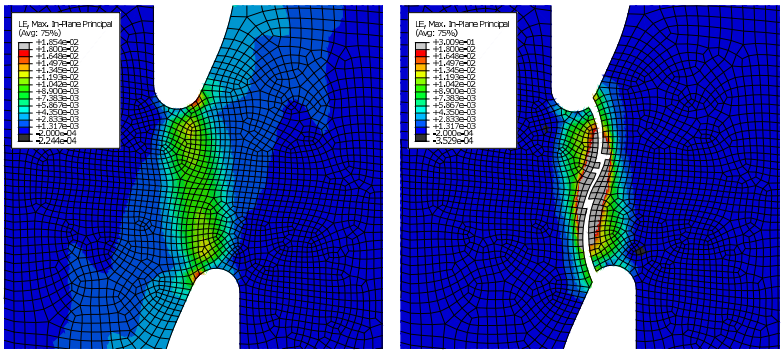

(a) *Step just before crack initiation.* (b) *Step just after crack initiation.*

Figure 7.1: *FE-simulation of shear notch geometry.*

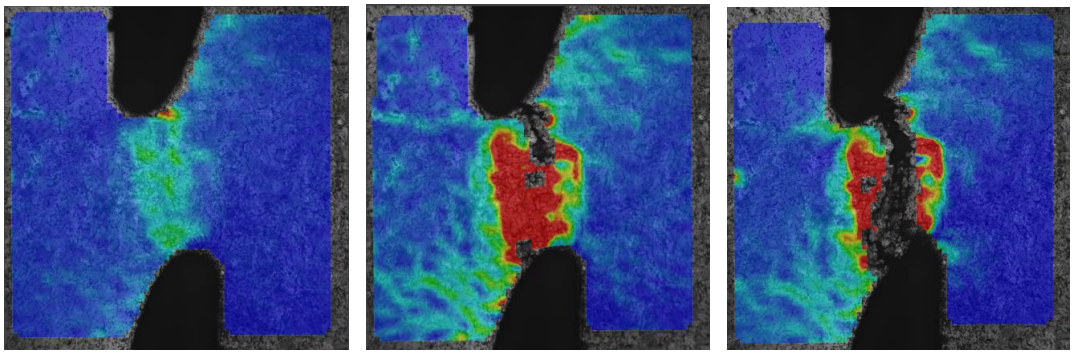

(a) *Image just before crack initiation.* (b) *Image during crack propagation.* (c) *Image after complete fracture.*

Figure 7.2: *Tensile test of shear notch geometry.*

7.4.2 Heterogeneous parameters

The number of experiments and FE-simulations performed have not given enough datapoints, i.e. fracture strain vs. stress triaxiality, for the parameter optimization to be effective. As seen in Figure 6.8, only two points are included into the optimization. One approach, which is used in [12], could be to set a very high fracture strain at the stress triaxiality value of -1/3, corresponding to a compression load case. This would give one additional point for optimization.

7.5 General discussion

7.5.1 Methodology

During this project the methodology of finding material parameters based on a combination of DIC and FE-analyses has been proved to be very useful. The methodology has up to this date seldom been applied, although there are examples of its use, such as in [2]. The use of DIC as a means of analyzing tensile test gives far more useful data from each test compared with conventional methods. It also adds an extra way to validate the FE-simulations by comparing the strain fields from the FE-simulations to those of the DIC-results.

7.5.2 Sustainability

The results contribute to a field of research which can potentially reduce the environmental impact of a product life cycle. In this case, a life cycle assessment of a cylinder block is used as an example. At the very start of the product life cycle, the design phase, there is a reduced need for the extensive testing and calibration of machining equipment. This decreases the use of raw material and energy. The energy consumption during manufacturing, when using CGI instead of e.g. aluminum is greatly reduced [26]. Although this potential energy saving might be diminished by the increased weight of a CGI component compared to aluminum, the energy saving is still positive when compared to other cast irons. The added durability of CGI can reduce fuel consumption when in use and increase the lifespan of e.g. a cylinder block.

8 Conclusions

- The Digital Image Correlation (DIC) technique has shown great potential, not only for the very specific needs of this project, but for many other applications where local strains are of interest as well. DIC is very well suited for validation of FE-simulations. The possibility to simulate strain fields and observe them in real world samples gives a simple and straight forward way to either confirm or disprove the results from a FE-simulation. At the same time doing this without any unnecessary impact on the testing due to DIC being a contact-less measuring technique makes it even better suited for validation.
- There is a lot to be gained by using FE-simulations for the study of CGI, and other materials, on both a macroscopic and microscopic level. Especially when the ability to simulate complex load cases, such as chip formation during machining, is refined and the parameters of the materials used are well defined and calibrated.
- The parameters for the Johnson-Cook model are possible to identify by a combination of experiments and simulation using the method described in this project.
- The homogeneous parameters of the Johnson-Cook model found are suitable for simulation of tensile test, the verification with shear test proved difficult because of the implementation of a simplified crack propagation model.
- The heterogeneous nature of CGI's microstructure influences the macroscopic response in fracture behavior and would suggest that a fracture model based on heterogeneous simulations is appropriate.
- The element removal technique is a simple and fast way to implement crack propagation in an explicit solver, but the crack propagation when using this method is not optimal. A more advanced method is needed if cracks are to be simulated without being influenced by mesh size and mesh geometry.

9 General recommendations and future work

9.1 Strain rate and temperature dependence

Due to time and equipment limitations, the strain rate and temperature dependence in the JC models were not investigated. This would be a useful investigation to perform since most machining processes occur at varying high strain rates and at high temperatures. As stated earlier, the resulting material parameters in this thesis were found via tests conducted at room temperature. The use of DIC in this process could be beneficial as the measuring apparatus does not need to be in contact with the specimen. Usually, strain gagues are used and mounted directly on the test specimen. The problem when using strain gauges in high temperature environments is that they tend to be influenced by the change in temperature making it difficult to assess the actual strain. Using DIC together with temperature controlled tensile testing equipment would be a suitable way to find the temperature dependence.

The strain rate's influence might be found by using a Split-Hopkinson pressure bar. This setup allows high strain rates deformations to be measured for tensile, compression and torsional testing.

9.2 Alternative specimen design

Some of the problems in this thesis concerned the test specimens and their design. Due to limitations in the manufacturing of the test specimen, the notch radii in the triangular and shear geometries have limitations to radii of $r > 0.2$ mm. This reduced the range of possible triaxiality values used in the optimization. In [21] a specimen design and loading equipment is shown which allows for a large variety of load cases from the same design. This also forces the crack to appear in the middle of the specimen, giving high degree of control of what stress triaxiality corresponds to what loading case.

9.3 Improved FE-modeling

A lot of problems that occurred in this work are related to the technique of simulating crack propagation in the FE-analyses. There exists a number of alternative techniques for simulation of crack propagation, e.g. XFEM, and it would be a good idea to investigate if any of these techniques are suitable for use in projects like this. Especially techniques that are less mesh dependent would be very desirable, as well as methodes that model the crack initiation and propagation in a more realistic and mesh independent way.

Other things that might improve the results are to use higher order elements in the analysis and also to try different mesh sizes. It is shown that the mesh size influence the stiffness of the structure. By trying to change the mesh size and fit the results, e.g. force-strain curves, to the results received in the DIC-analyses, a more realistic simulation might be obtained.

9.4 Tensile tests and DIC-analysis

For the heterogeneous approach, problems occurred when trying to compute the strain in the microstructure with the DIC-technique. These problems were related to the technique used to receive the random pattern needed for the analysis, as described in subsection 3.3.1. When the toner powder has been applied, it is hard to distinguish between dark spots of toner powder and dark spots of graphite. This was solved by capturing an image of the microstructure, before toner powder was applied, at the location where the microscope camera was to capture images. By manually fitting the image of the microstructure with those taken from the camera with the toner powder applied to the surface, it was possible to get a quite good idea of what was graphite and what was toner powder. However, to make this process a little bit easier, it could be possible to put some marking into the microstructure using e.g. microindentation which leaves distinct markings that are easy to identify but at the same do not cause to high stress concentrations.

9.5 FEA with DIC

The computer software that comes with the Aramis-system has the possibility to import data-sets from a number of different FEA-softwares [20]. This possibility could be worth looking into as it might be easier to compare the FE-simulations with the DIC-analyses using only one software. It might also give possibilities to compare in more ways than the two used in this project, force vs. strain curves and strain field images.

References

[1] S. Dawson. Compacted Graphite Iron: A Material Solution for Modern Diesel Engine Cylinder Blocks and Heads. *68th WFC - World Foundry Congress*. Chennai, India: SinterCast, (2008), pp. 93–99.

[2] V. Tarigopula et al. A Study of Large Plastic Deformations in Dual Phase Steel Using Digital Image Correlation and FE Analysis. *Experimental Mechanics* **48** (2008), pp. 181–196.

[3] SP Technical Research Institute of Sweden. *Non-contact deformation measurement*. Jan. 2012. URL: `http://www.sp.se/en/index/resources/contact-freedeformation/Sidor/default.aspx`.

[4] G. Ljustina. *Modeling and simulation of CGI machining on microstructure level*. 2010:08. LicEng thesis. Department of Applied Mechanics Chalmers University of Technology Göteborg, Sweden, 2010.

[5] G. R. Johnson and W. H. Cook. A constitutive model and data for metals subjected to large strains, high strain rates and high temperatures. *Proceedings of the 7th International Symposium on Ballistics*. Vol. 547. the Hague, Netherlands, (1983), pp. 541–547.

[6] Dassault Systèmes. *Abaqus Unified FEA*. May 2012. URL: `http://www.3ds.com/products/simulia/portfolio/abaqus/overview/`.

[7] MathWorks. *Matlab Documentation*. May 2012. URL: `http://www.mathworks.se/help/techdoc/`.

[8] A. Malakizadi and M. a. Rezazadeh Bina. Flow stress determination of 1080 Carbon steel using inverse modeling of orthogonal cutting. Private communication. (2012).

[9] S. Dawson. Compacted graphite iron: mechanical and physical properties for engine design. *Materials in Powertrain VDI*. Dresden, Germany: SinterCast Technical Publication, (1999), pp. 93–99.

[10] K. Varghese. *Machining of Compacted Graphite Iron (CGI) and Spheroidal Graphite Iron (SGI): A fundamental study of tribological issues and progressive cutting tool wear*. Salt Lake City, UT, USA: The University of Utah, (2008).

[11] E. Abele, A. Sahm, and H. Schulz. Wear Mechanism when Machining Compacted Graphite Iron. *Manufacturing Technology* **51** (2002), pp. 53–56.

[12] X Teng and T Wierzbicki. Evaluation of six fracture models in high velocity perforation. *Engineering Fracture Mechanics* **73** (2006), pp. 1653–1678.

[13] L. Schwer. Optional Strain-Rate Forms for the Johnson Cook Constitutive Model and the Role of the Parameter ϵ_0. *6th European LS-DYNA Users' Conference*. Göteborg, Sweden: Engineering Research AB, (2007).

[14] R. Larsson, M. Fagerström, and G. Ljustina. Hypo– and hyperinelasticity applied to modeling of compacted graphite iron machining simulations. *Proceedings of the 24th nordic seminar on computational mechanics*. Helsinki, Finland: Aalto University School of Engineering, (2011), pp. 59–62.

[15] J Mediavilla, R. H. J. Peerlings, and M. G. D. Geers. A nonlocal triaxiality-dependent ductile damage model for finite strain plasticity. *Computer Methods in Applied Mechanics and Engineering* **195** (2006), pp. 4617–4634.

[16] T. Belytschko, W. Liu, and B. Moran. *Nonlinear finite elements for continua and structures*. Wiley. Chichester, England, 2000.

[17] L. Olovsson, K. Simonsson, and M. Unosson. Selective mass scaling for explicit finite element analyses. *International Journal for Numerical Methods in Engineering* **63** (2005), pp. 1436–1445.

[18] *Abaqus 6.10 - Abaqus/CAE User's Manual*. 6.10. Dassault Systemes. Providence, RI, USA, (2012).

[19] T. Sjögren, SP Technical Research Institute of Sweden. Test preparation of CGI. Private communication. (2012).

[20] GOM. *ARAMIS Software*. May 2012. URL: `http://www.gom.com/3d-software/aramis-software.html`.

[21] D. Mohr and S. Henn. Calibration of Stress-triaxiality Dependent Crack Formation Criteria: A New Hybrid Experimental–Numerical Method. *Experimental Mechanics* **47** (2007), pp. 805–820.

[22] National Institute of Standards and Technology. *OOF: Finite Element Analysis of Microstructures*. May 2012. URL: http://www.ctcms.nist.gov/oof/oof2/.

[23] N. Narasaiah and K. Ray. Small crack formation in a low carbon steel with banded ferrite–pearlite structure. *Materials Science and Engineering* **392** (2005), pp. 269–277.

[24] Qimtek. *Trådgnistning*. Text in Swedish. June 2012. URL: http://www.qimtek.se/category/tradgnistning-27.html.

[25] W. M. Mohammed El Sabagh. The Effect of Compacted Graphite Iron Microstructure on Fracture and Machining. *DigitalCommons McMaster University,* Hamilton, ON, Canada 6225 (2011).

[26] K. D. Peasle. *A Comparative Life Cycle Assessment of Cast Aluminum, Cast Iron, and Forged Steel Automotive Parts*. May 2012. URL: http://www.autosteel.org/~/media/Files/Autosteel/GreatDesignsinSteel/GDIS2008/27-GreenhouseGasComparisonofSteeringKnuckles.ashx.

A Test specimen drawings

A.1 Shear notch geometry

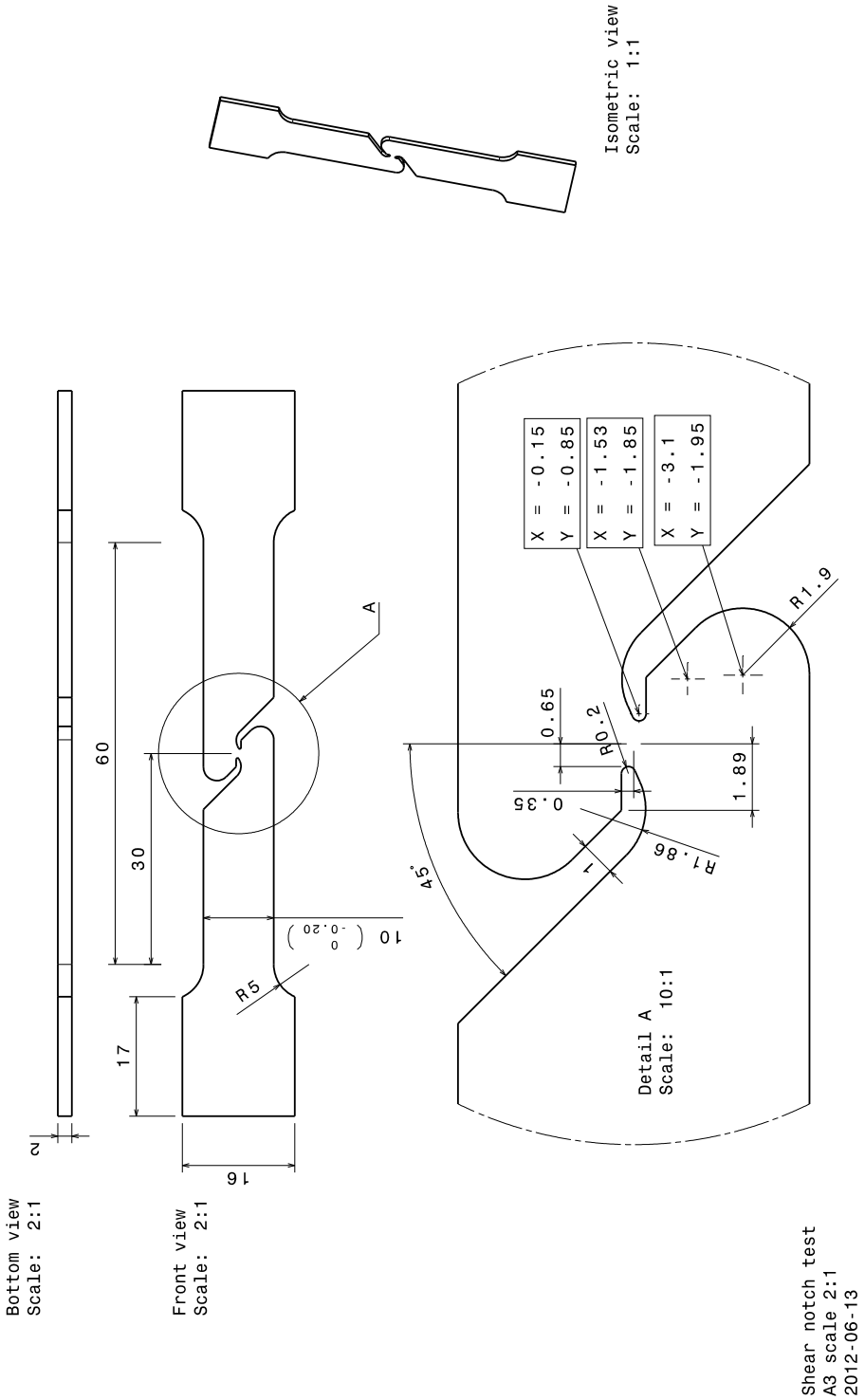

A.2 Large radius notch geometry

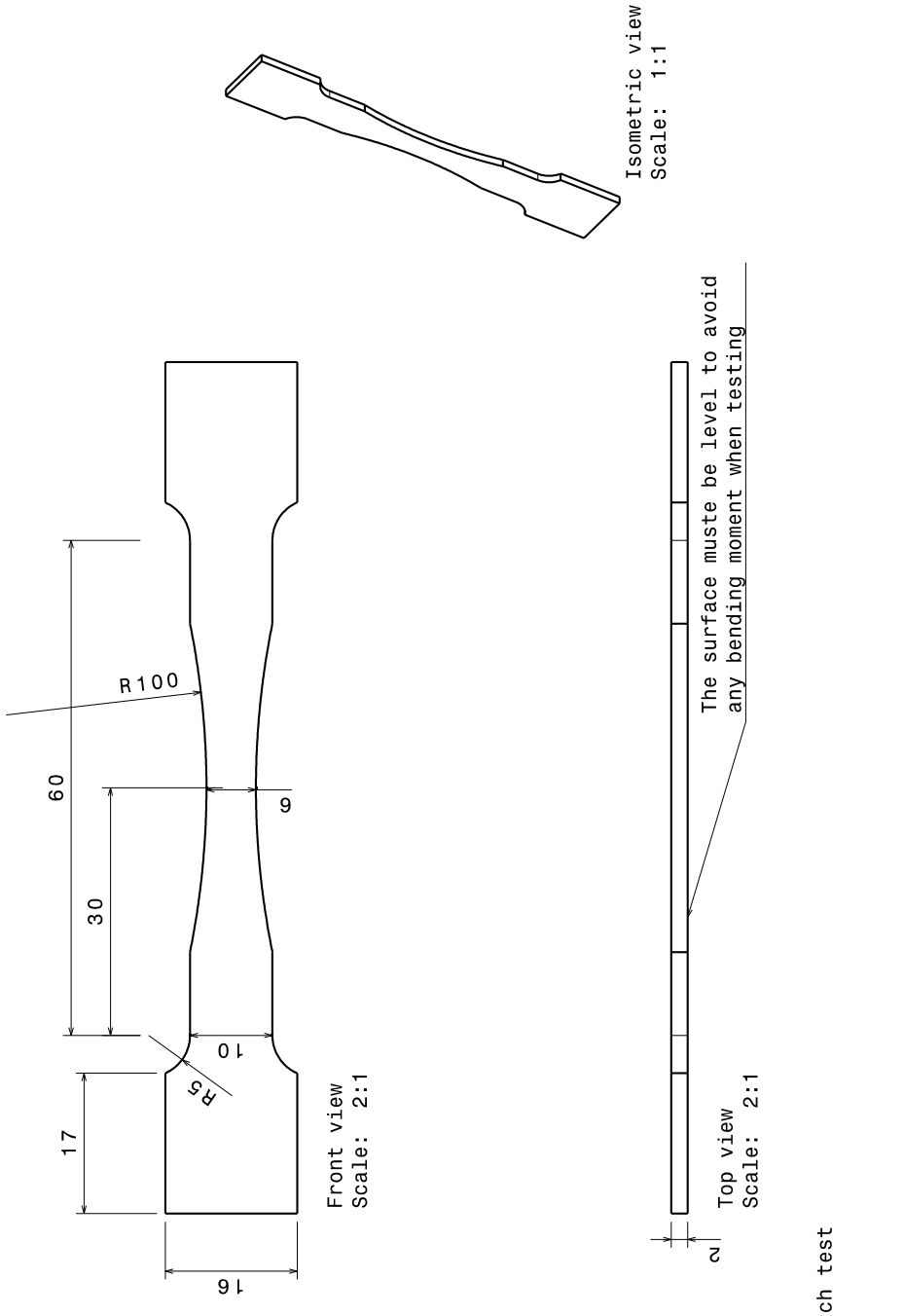

A.3 Circular notch geometry

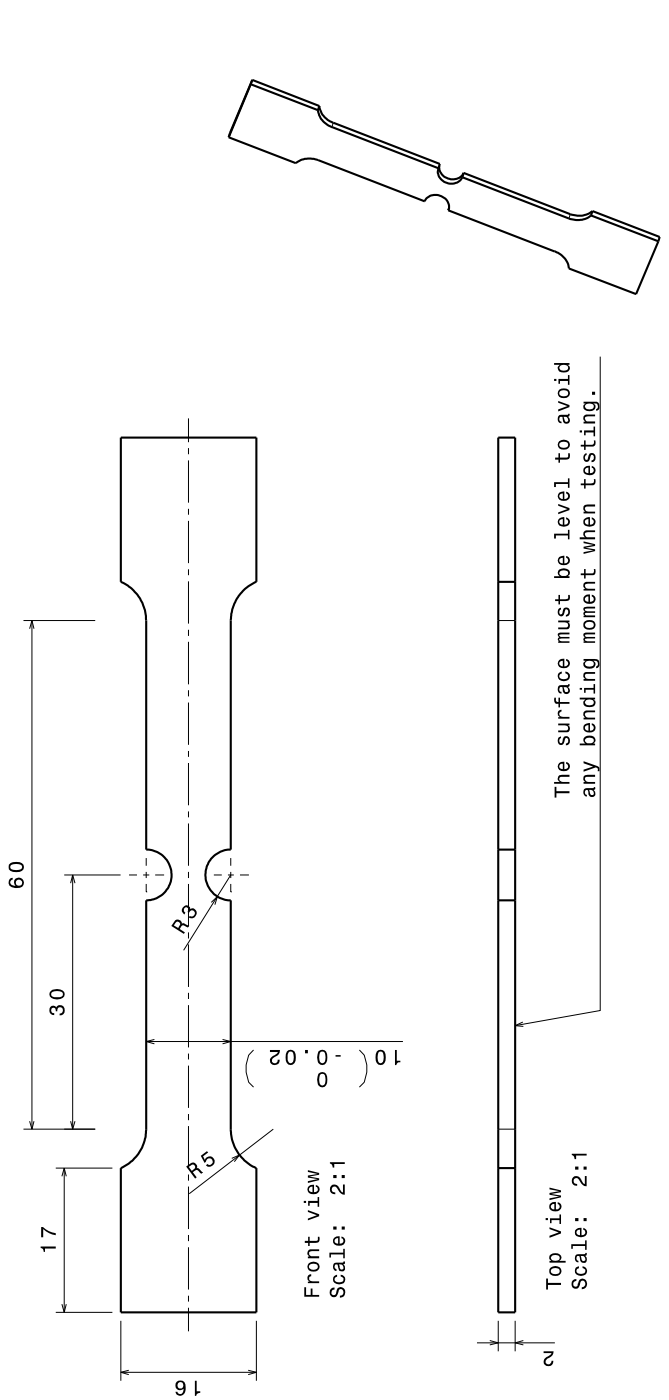

Circular notch test
A3 Scale 1:2
2012-01-25

A.4 Triangular notch geometry

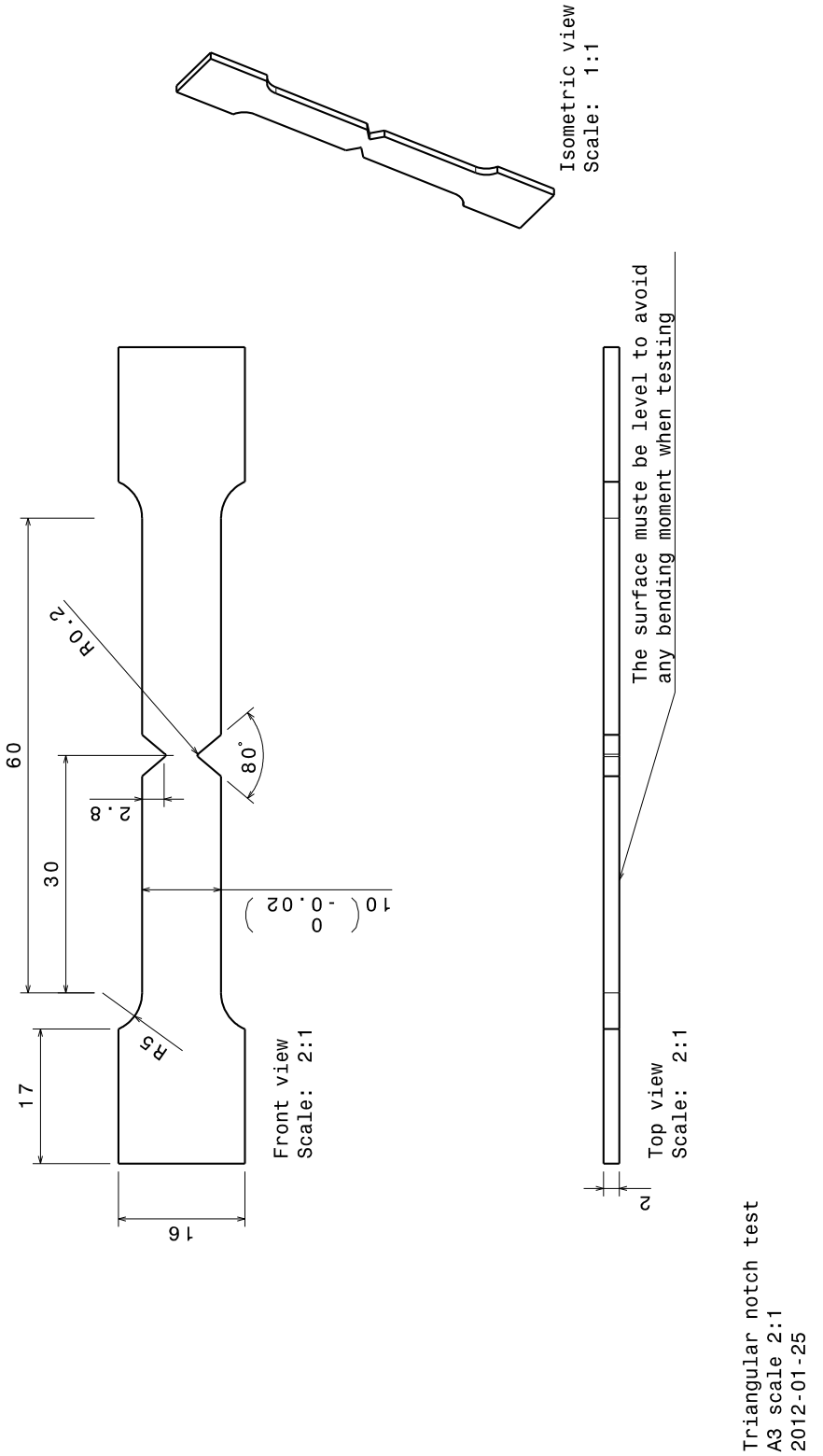

B Matlab Codes

B.1 ADdataFromAramisFinal.m

```
%-----------------------ADdataFromAramisFinal.m-------------------------
% Uses load and strain data from aramis to find fracture strain limit.
%
% Input:   filePath
%          loadFile in format: [pointStage, force]
%          strainFile in format: [pointStage, LL1, LL2, LL3, LS1, LS2, LS3]
%
% Output:     fractureStrain = Fracture strain for all test samples.
%             fractureForce = Fracture force for all test samples.
%
%
%
% Created by:   Peter Hellström
%               Kim Olander
%
%
% Date:         2012-04-02
% Edit:         2012-06-12
%-------------------------------------------------------------------------
close all; clc; clear all;
area=6*2; %Cross section area [mm^2]
h = figure(1);
type='waist';
iter=1;
for testLoop=1:5;
    filePath='.\TextData_Final\';
    testNr=num2str(testLoop)
    % Load-file
    fileNameForce=[type '_Prov' testNr '_LoadStage'];
    indataForce=importdata([filePath fileNameForce],';' ,3);
    stress=-indataForce.data(:,2)*1E3/area; %Name force*kN/(area)
    % Strain-file
    fileNameStrain=[type '_Prov' testNr '_strainStage_midlength'];
    indataStrain=importdata([filePath fileNameStrain],';' ,3);
    % The following for loop cycles through each strain gauge and plots the
    % result as well as detects the fracture strain and fracture stress
    [~,maxInd]=max(stress);
    fractPoint=[];
    for i=1:size(indataStrain.data,2)-1
        % The data read from file is set to current strain
        currentStrain=indataStrain.data(1:maxInd,i+1);
        plot(currentStrain,stress(1:maxInd),'r')
        hold on
        % Find fracture strain
        fractPoint=[fractPoint; [currentStrain(maxInd) stress(maxInd)]];
        fractPointAll((testLoop-1)*3+i,:)=[currentStrain(maxInd) stress(maxInd)];
    end
    % Average of each fracture strain triplettes
    avgLL=sum(fractPoint(1:3,1),1)/3;
    if size(indataStrain.data,2)-1 > 3
        avgLS=sum(fractPoint(4:6,1),1)/3;
```

```
    end
    %% Plotting and axis
    xlabel('\epsilon [log]')
    ylabel('Stress [MPa]')
    axis([0 0.025 0 450])
    title({'Stress vs strain'; 'for large radius notch'})
    %% Adds to output for all types and tests
    if size(indataStrain.data,2)-1==3
        fractureStrain(iter)=avgLL;
        fractureForce(iter)= stress(maxInd);
        LLorLS{iter}='LS';
        iter=iter+1;
    elseif size(indataStrain.data,2)-1==6
        fractureStrain(iter)=avgLS;
        fractureForce(iter)= stress(maxInd);
        LLorLS{iter}='LL';
        iter=iter+1;
    else
        error('No LS error in LL???')
    end
end
```

B.2 EMakingFinal.m

```
%%----------------------------EMakingFinal.m-----------------------------
% Purpose: This programe is created to compute Young's modulus E and Yield
% stress from a stress-strain curve. The user are given two options to pick
% points in the stress-strain curve. The first point is used to compute E
% by calculating the slope between this point and (0,0).
%
% Created by:   Kim Olander
%               Peter Hellström
%
% Date: 2012-03-06
% Last Edit: 2012-06-12
%-----------------------------------------------------------------------------
clear variables; close all; clc; format shortg
%% Load and plot stress-strain curve
% data_real=load('extrData_scaled_Black.txt');
% data_real=load('cleanData_Midja_2.txt');
data_real=load('averageStrainVsStressWaist.mat');
% data_real=load('waistLongGaugeAvgStrainStress.mat');    % New longer strain gauges
% data_real=data_real.avgStrainVsStress; %Data from .mat is array this sets it to variable
data_real=load('waistMidGaugeAvgStrainStress.mat');    % New semilong strain gauges
data_real=data_real.avgStrainVsStress;
figure(1)
plot(data_real(1:end,1), data_real(1:end,2),'-r')
xlabel('\epsilon')
ylabel('\sigma [MPa]')
title('Stress as a function of strain')
%% Compute stuff from data points
% Extract data in elastic region, need to check where to sample before
% running the program.
Val=ginput(1);
data_E=data_real(data_real(:,2) < Val(1,2),:);
```

```
E1_End=(data_E(end,2)-data_E(1,2))/(data_E(end,1)-data_E(1,1));
x=linspace(data_E(1,1), data_E(end,1));
figure(2)
plot(data_E(:,1), data_E(:,2),'r-')
hold on
plot(x,E1_End*x)
figure(1)
hold on
x2=linspace(0,0.01,1000);
huck=x2*E1_End;
plot(x2,huck)
axis([0 0.02 0 500])
%% Print results to screen and figure
E1_End=E1_End/1E3;
Young=['Young''s modulus: ', num2str(E1_End),' GPa'];
FractSig=['Fracture stress :~ ' ,num2str(data_real(end,2)),' MPa'];
FractEps=['Fracture strain :~ ' ,num2str(data_real(end,1)*100),' %  (', num2str(data_real(end,1)),')'];
text(0.006, 200, Young); text(0.006, 180, FractSig); text(0.006, 160, FractEps);
disp(Young); disp(FractSig); disp(FractEps)
```

B.3 ParamOptimJCModelHetero.m

```
%%--------------------ParamOptimJCModelHetero.m--------------------------
% Purpose: This program is used to find parameters in the Johnson-Cook
% fracture model based on data from the DIC-system Aramis at SP.
% The program uses functions from Matlabs optimization toolbox to find the
% parameters with the nonlinear least square method.
%
% JC-model: Plasitcity
%           sig_0  = A + B*(eps_h)^n
%           Hardening
%           epsi_f = d1 + d2*exp(d3*(-p/sig_e^vm))
%
% Written by: Kim Olander
%             Peter Hellström
%
% Date: 2012-04-19
% Last Edit: 2012-06-11
%-------------------------------------------------------------------------
clear variables; close all; clc;
%% Pre-processing
format shortg
d0=[1 1 1];   % Initial guess
lb=[0 0 0];    % Lower bound
ub=[1000 1000 1000];     % Upper bound
PrecondBandWidth_Data=1000; % See doc for more info.
%% Triaxiality and fracture strains
% Data taken from Abaqus and DIC analyses.
global triax epsiFrac
triax=[0.404 0.404 0.345];
epsiFrac=[0.00654 0.00654 0.00964];
%% This is an auto generated MATLAB file from Optimization Tool.
% Start with the default options
options = optimset;
% Modify options setting
```

```
options = optimset(options,'Display', 'off');
options = optimset(options,'PlotFcns', {  @optimplotx @optimplotresnorm @optimplotstepsize @optimplotfi
options = optimset(options,'Algorithm', 'trust-region-reflective');
options = optimset(options,'Diagnostics', 'off');
options = optimset(options,'Jacobian', 'off');
options = optimset(options,'PrecondBandWidth', PrecondBandWidth_Data);
[d,resnorm,residual,exitflag,output,lambda,jacobian] = ...
    lsqnonlin(@JCFractureFunction,d0,lb,ub,options);
%% Post-processing
% Plot function with optimized parameters and original data points.
tria=linspace(-1/3,0.8);
epsi=d(1)+d(2)*exp(-d(3)*tria);
figure(10)
hold on
plot(tria, epsi,'k',triax, epsiFrac,'*k')
xlabel('Triaxility: -P/\sigma_{vM}^e')
ylabel('\epsilon_f')
legend('Function with optimized parameters','Data points')
axis([-0.2 1 -0.001 0.08])
title('Fracture strain as function of triaxility (Heterogeneous approach)')
```

B.4 ParamOptimJCModelsHomo.m

```
%%----------------------ParamOptimJCModelsHomo.m--------------------------
% Purpose: This program is used to find parameters in the Johnson-Cook
% hardening and fracture model based on data from the DIC-system Aramis at
% SP. Program uses functions from Matlabs optimization toolbox to find the
% parameters with the nonlinear least square method.
%
% JC-model: Plasitcity
%           sig_0  = A + B*(eps_h)^n
%           Hardening
%           epsi_f = d1 + d2*exp(d3*(-p/sig_e^vm))
%
% Written by: Kim Olander
%             Peter Hellström
%
% Date: 2012-04-19
% Last Edit: 2012-06-12
%------------------------------------------------------------------------
clear variables; close all
% Choose which model på find parameters for
model='Fracture'; % 'Fracture' 'Hardening'
switch model
    case 'Hardening' % Find parameters for hardening model.
        %% Pre-processing
        x0=[100 0.25];   % Initial guess
        lb=[-1000 -1000];    % Lower bound
        ub=[10000 10000];     % Upper bound
        PrecondBandWidth_Data=1000; % See doc for more info.
        % Set global parameters, also used in the objective function for the
        % optimization toolbox
       global E epsiPlast sigmaPlast A
       % Define young's modulus and yield stress (A) based on results from
       % E_making_v2.m
```

```
        E=1.225E5; % Approximated from stress-strain curve
        A=260;  % Should be the yield stress
        % Load stress-strain curve.
        % data=[strain, stress]
        data=load('averageStrainVsStressWaist.mat');
        data=data.avgStrainVsStress; %Data from .mat is array this sets it to variable
        epsi=data(1:1:end,1); % Strain values
        sigma=data(1:1:end,2);    % Stress values
        indElast=find(sigma<=A); % Find values in elastic region
        indPlast=find(sigma>A);  % Find values in plastic region, used in optimization routine
        epsiPlast=epsi(indPlast);   % Extract plastic values
        sigmaPlast=sigma(indPlast); % Extract plastic values
                %% This is an auto generated MATLAB file from Optimization Tool.
        % Start with the default options
        options = optimset;
        % Modify options setting
        options = optimset(options,'Display', 'off');
        options = optimset(options,'PlotFcns', {  @optimplotx @optimplotresnorm @optimplotstepsize @opt
        options = optimset(options,'Algorithm', 'trust-region-reflective');
        options = optimset(options,'Diagnostics', 'off');
        options = optimset(options,'Jacobian', 'off');
        options = optimset(options,'PrecondBandWidth', PrecondBandWidth_Data);
        [x,resnorm,residual,exitflag,output,lambda,jacobian] = ...
            lsqnonlin(@JCHardeningFunction,x0,lb,ub,options);
                %% Plot solution and original data
        figure
        plot(epsi,sigma,'-k') % Plot original data
        hold on
        sigmaPlot2=A + x(1).*(epsiPlast-sigmaPlast./E).^x(2); % Compute stress from JC-model with optim
        plot(epsiPlast,sigmaPlot2,'--k')
        xlabel('\epsilon [-]')
        ylabel('\sigma [MPa]')
        plot(epsi(indElast), E*epsi(indElast),'-.k') % Plot stress-strain in elastic region with calcul
        legend('Original data','JC hardening with params','Elastic region, Hooke''s law','location','So
    case 'Fracture'
        %% Pre-processing
        format shortg
        d0=[1 1 1];   % Initial guess
        lb=[0 0 0];    % Lower bound
        ub=[10 10 10];     % Upper bound
        PrecondBandWidth_Data=1000; % See doc for more info.
        global triax epsiFrac
        % Order: Shear Unnotched Circnotch Trianotch
        ShearStrains=[0.048328 0.050423 0.067099 0.062585];
        meanShear=mean(ShearStrains);
        WaistStrains=[0.0167 0.0164 0.0170 0.0175 0.0172];
        meanWaist=mean(WaistStrains);
        CircStrains=[0.0218 0.0160 0.0125 0.0172 0.0187];
        meanCirc=mean(CircStrains);
        TriStrains=[0.0081 0.0080 0.0125 0.0156 0.0165];
        meanTri=mean(TriStrains);
        triax1=[0.048 0.33 0.467 0.603]; % Triax from abaqus simulation with params from Gorans lic.
%       triax1=[0.047077 0.33845 0.467 0.60292]; % Triax from new abaqus simulations with updated param
        %------------------- Run with all values -----------------------
        triax=[triax1(1)*ones(1,length(ShearStrains)) triax1(2)*ones(1,length(WaistStrains)) triax1(3)*
             triax1(4)*ones(1,length(TriStrains))];
```

```
        epsiFrac=[ShearStrains WaistStrains CircStrains TriStrains];
         %------------------ Run with mean values ----------------------
%         epsiFrac=[meanShear meanWaist meanCirc meanTri];
%         triax=triax1;
        %% This is an auto generated MATLAB file from Optimization Tool.
        % Start with the default options
        options = optimset;
        % Modify options setting
        options = optimset(options,'Display', 'off');
        options = optimset(options,'PlotFcns', {  @optimplotx @optimplotresnorm @optimplotstepsize @opt
        options = optimset(options,'Algorithm', 'trust-region-reflective');
        options = optimset(options,'Diagnostics', 'off');
        options = optimset(options,'Jacobian', 'off');
        options = optimset(options,'PrecondBandWidth', PrecondBandWidth_Data);
        [d,resnorm,residual,exitflag,output,lambda,jacobian] = ...
            lsqnonlin(@JCFractureFunction,d0,lb,ub,options);
        %% Post-processing
        tria=linspace(-1/3,0.8);
        epsi=d(1)+d(2)*exp(-d(3)*tria);
        figure(10)
        hold on
        plot(tria, epsi,'b',triax, epsiFrac,'dr')
        xlabel('Triaxiality')
        ylabel('\epsilon_f [-]')
        legend('Function with optimized parameters','Data points')
        axis([-0.2 1 -0.001 0.08])
        box on
end
```

B.5 JCFractureFunction.m

```
function f=JCFractureFunction(d)
%-------------------------JCFractureFunction.m-----------------------------
% Functionfile used for finding parameters in the Johnson-Cook fracture
% model.
%
% Created by:   Kim Olander
%               Peter Hellström
%
% Date:         2012-06-12
%------------------------------------------------------------------------
global E epsiY data epsi sigma epsiPlast sigmaPlast triax epsiFrac
% d(1)=d_1, d(2)=d_2, d(3)=d_3
f=d(1)+d(2)*exp(-d(3)*triax)-epsiFrac;
```

B.6 JCHardeningFunction.m

```
function f=JCHardeningFunction(d)
%-------------------------JCHardeningFunction.m---------------------------
% Functionfile used for finding parameters in the Johnson-Cook hardening
% model.
%
% Created by:   Kim Olander
%               Peter Hellström
%
```

```
% Date:         2012-06-12
%-------------------------------------------------------------------------
global E epsiPlast sigmaPlast A
% d(1)=B d(2)=n
f = A + d(1).*(epsiPlast-sigmaPlast./E).^d(2) - sigmaPlast;
```

B.7 AbaqusShearEdtv2.m

```
%----------------------------AbaqusShearEdtv2.m----------------------------
% Purpose: Compute fracture shear strain based on deformation of a square.
% Information about the square deformation comes from Aramis calculations
% at SP. The square is placed over the crack zone. Data about the movement
% of the corner points is recorded and loaded into this program.
%
% Created by:   Peter Hellström
%               Kim Olander
%
% Date:              2012-05-09
% Last Edit:         2012-06-11
%-------------------------------------------------------------------------
close all; clc; clear all;
%% Import data from Abaqus textfiles
force=importdata('./shearDataMeasure120602/shear_RF.txt');
Points=importdata('./shearDataMeasure120602/shear_COORD.txt');
%% Force
% stress=k*force;
figure(1); plot(force,'-*')
title('Force vs time'); xlabel('Time [s]'); ylabel('Force [N]')
%% Compute shear strain
[~,I_force]=max(force);    % Find failure index
gam1=zeros(size(Points,1),1); gam2=zeros(size(Points,1),1);
gam3=zeros(size(Points,1),1); gam4=zeros(size(Points,1),1);
for i=1:size(Points,1)
    % Compute vectors at square side
    v12(i,:)=Points(1,3:4)-Points(1,1:2);
    v12_prim(i,:)=Points(i,3:4)-Points(i,1:2);
    v23(i,:)=Points(1,5:6)-Points(1,3:4);
    v23_prim(i,:)=Points(i,5:6)-Points(i,3:4);
    v34(i,:)=Points(1,7:8)-Points(1,5:6);
    v34_prim(i,:)=Points(i,7:8)-Points(i,5:6);
    v41(i,:)=Points(1,1:2)-Points(1,7:8);
    v41_prim(i,:)=Points(i,1:2)-Points(i,7:8);
    % Compute angles at lower left corner using scalar product
    alpha1(i,1)=acos(dot(v12(i,:),v12_prim(i,:))/(norm(v12(i,:))*norm(v12_prim(i,:))));
    beta1(i,1)=acos(dot(v41(i,:),v41_prim(i,:))/(norm(v41(i,:))*norm(v41_prim(i,:))));
    % Compute angles at upper left corner using scalar product
    alpha2(i,1)=acos(dot(v23(i,:),v23_prim(i,:))/(norm(v23(i,:))*norm(v23_prim(i,:))));
    beta2(i,1)=acos(dot(v12(i,:),v12_prim(i,:))/(norm(v12(i,:))*norm(v12_prim(i,:))));
    % Compute angles at lower right corner using scalar product
    alpha3(i,1)=acos(dot(v34(i,:),v34_prim(i,:))/(norm(v34(i,:))*norm(v34_prim(i,:))));
    beta3(i,1)=acos(dot(v23(i,:),v23_prim(i,:))/(norm(v23(i,:))*norm(v23_prim(i,:))));
    % Compute angles at upper right corner using scalar product
    alpha4(i,1)=acos(dot(v41(i,:),v41_prim(i,:))/(norm(v41(i,:))*norm(v41_prim(i,:))));
    beta4(i,1)=acos(dot(v34(i,:),v34_prim(i,:))/(norm(v34(i,:))*norm(v34_prim(i,:))));
end
```

```
gam1=alpha1+beta1;
gam2=alpha2+beta2;
gam3=alpha3+beta3;
gam4=alpha4+beta4;
% Plot quadrangles deformation and some other stuff
figure(2)
for i=1:size(Points,1)
    subplot(2,2,1)
    plot(Points(i,[1,3]), Points(i,[2,4]),'r-*')
    hold on
    plot(Points(i,[3,5]), Points(i,[4,6]),'r-*')
    plot(Points(i,[5,7]), Points(i,[6,8]),'r-*')
    plot(Points(i,[7,1]), Points(i,[8,2]),'r-*')
    % Original position
    plot(Points(1,[1,3]), Points(1,[2,4]),'r-*')
    plot(Points(1,[3,5]), Points(1,[4,6]),'r-*')
    plot(Points(1,[5,7]), Points(1,[6,8]),'r-*')
    plot(Points(1,[7,1]), Points(1,[8,2]),'r-*')
    hold off
    title('Deformation quadrangle')
    % Plot of force
    subplot(2,2,2)
    plot(force(1:i),'-*')
    title('Force vs time')
    xlabel('Time [s]')
    ylabel('Force [N]')
    axis([0 size(Points,1) -100 1100])
    % Plot of angle change
    subplot(2,2,3)
    plot(1:i,gam1(1:i),'r--',1:i,gam2(1:i),'b--',1:i,gam3(1:i),'b.-'...
        ,1:i,gam4(1:i),'r.-')
    title('Angles vs time')
    xlabel('Time [s]')
    ylabel('Angle')
    legend('\gamma1','\gamma2','\gamma3','\gamma4', 'location', 'NorthWest')
    pause(1/20)
end
% Compute shear strain
for i=1:size(Points,1)
    ShearStrainTensor=zeros(3); ShearStrainTensor(1,2)=mean([gam2(i) gam4(i)]/2);
    ShearStrainTensor(2,1)=mean([gam2(i) gam4(i)]/2);
    epsi(i)=sqrt((2/3)*sum(sum(ShearStrainTensor.*ShearStrainTensor)));
end
% Find indice for maximum force.
Y=0;
while ~Y
    Failstrains=[gam1(I_force) gam2(I_force) gam3(I_force) gam4(I_force)]
    if sum(isnan(Failstrains))>0
        I_force=I_force-1
    else
       Y=1;
    end
end
epsi_F=epsi(I_force);
```

C Tensile testing machine specifications

Motor: ABB Servo Motor 8C
Gearbox: Neugart PLE80 1:8
Load cell: Burster 8524-6010
Lens: Schneider Kreuznach 50mm f2.8
Sensor: Gom CCD-4000G
Image processor: Gom Aramis